Experimental Investigation and Development of Finite Element Model for Knife and Spike Impact

by

Erblina Vokshi

A Thesis Presented in Partial Fulfillment
of the Requirements for the Degree
Master of Science

Approved December 2011 by the
Graduate Supervisory Committee:

Subramaniam Rajan, Chair
Narayanan Neithalath
Barzin Mobasher

ARIZONA STATE UNIVERSITY

May 2012

ABSTRACT

Ultra-concealable multi-threat body armor used by law-enforcement is a multi-purpose armor that protects against attacks from knife, spikes, and small caliber rounds. The design of this type of armor involves fiber-resin composite materials that are flexible, light, are not unduly affected by environmental conditions, and perform as required. The National Institute of Justice (NIJ) characterizes this type of armor as low-level protection armor. NIJ also specifies the geometry of the knife and spike as well as the strike energy levels required for this level of protection. The biggest challenges are to design a thin, lightweight and ultra-concealable armor that can be worn under street clothes.

In this study, several fundamental tasks involved in the design of such armor are addressed. First, the roles of design of experiments and regression analysis in experimental testing and finite element analysis are presented. Second, off-the-shelf materials available from international material manufacturers are characterized via laboratory experiments. Third, the calibration process required for a constitutive model is explained through the use of experimental data and computer software. Various material models in LS-DYNA for use in the finite element model are discussed. Numerical results are generated via finite element simulations and are compared against experimental data thus establishing the foundation for optimizing the design.

To My Vokshi and Shropshire Family…

ACKNOWLEDGEMENTS

I express my sincere gratitude to my advisor and committee chair, Dr. Subramaniam D. Rajan, for challenging, guiding, and supporting me throughout the course of my Master's degree. I would also like to extend thanks to Dr. Barzin Mobasher and Dr. Neithalath for being in my thesis committee. I would like to thank Armor Designs Inc., Phoenix, for providing financial support for this research. I greatly appreciate the help provided by Peter Goguen and Dr. Dallas Kingsbury for all the help and guidance regarding laboratory work. Thanks are also extended to the Fulton Undergraduate Research Initiative students Michael Mast and Linda Kuenzi for their help in the laboratory and processing experimental data needed for my research. I am very glad to have moral support from all my friends. I would like to acknowledge all my classmates and colleagues, especially Jon Fein, Aditya Vaidya, Arumugam Deivanayagam, and Canio Hoffarth. I would also like to express my gratitude to all the CEE and ASU administrative staffs for their kind help and support. Last and the most important I would like to thank my father Sadik Vokshi, my mother Ferdeze Vokshi, my sister Bujeta Vokshi, and my brother Granit Vokshi whose support and sacrifice have brought me to this place. Also my Shropshire family, especially Dian Shropshire who has not only provided a home for me during my Master's degree but also has made me feel like I'm her granddaughter. I will eternally be thankful and appreciative.

TABLE OF CONTENTS

Page

LIST OF TABLES viii

LIST OF FIGURES ix

ABBREVATIONS xii

CHAPTER

1. INTRODUCTION 1

1.1 Literature review 2

1.1.1 Puncture testing literature review 2

1.1.2 Stab Resistance Materials Literature Review 5

1.1.3 Modeling ballistic impacts literature review 6

1.2 Thesis Objectives & Overview 7

1.2.1 Thesis Objectives 7

1.2.2 Thesis Overview 9

2. ANALYSIS OF EXPERIMENTAL DATA 11

2.1 Statistical tests 11

2.2 Determination of number of samples in an experiment 12

2.3 Smoothing techniques in experimental data 14

2.3.1 Moving Median Smoothing Technique 14

2.3.2 Moving Average Filters 14

2.4 Regression analysis 15

2.4.1 One-variable regression analysis 15

2.4.1.1 Linear and Polynomial Fitting 16

CHAPTER Page

2.4.1.2 Exponential fitting 19

2.4.1.3 Logarithmic fitting 19

2.4.2 Correlation Coefficient 20

2.4.3 Multi-variable regression analysis 21

2.4.3.1 Goodness of fit 23

3. MATERIAL MODEL DESCRIPTIONS AND EXPERIMENTAL TESTS 27

3.1 Material Descriptions 27

3.1.1 Steel Material 27

3.1.2 Steel Material Models in LS-DYNA 27

3.1.3 Foam material 28

3.1.2 Foam Material Models in LS-DYNA 28

3.1.5 Dry fabrics material 30

3.1.6 Composite material models considered in LS-DYNA 35

3.2 Tension tests for fiber resin composites 38

3.2.1 Objective 38

3.2.2 Apparatus and Experimental Setup 39

3.2.3 Test Procedure 41

3.2.4 Tension Properties Calculations 41

3.2.5 GN2118 Results 42

3.2.6 AS299 Results 43

CHAPTER Page

3.3 Foam Compression Test 43

3.3.1 Objective 44

3.3.2 Apparatus and Experimental Setup.....44

3.3.5 Results.....45

3.4 Drop-sphere Test as Means of Validation of Material Models48

3.4.1 Overview and significance.....48

3.4.2 Apparatus 48

3.4.3 Test Procedure 49

3.4.4 Processing Experimental Data 49

3.4.5 Results for steel.....50

3.4.6 Results for foam.....50

3.4.7 Results for GN2118 and AS299 51

3.5 Knife and Spike Test.....52

3.5.1 Objective 52

3.5.2 Apparatus and Test Setup 53

3.5.3 Results and Discussion 57

3.6 Discussion of the experimental test results.....59

4. FINITE ELEMENT ANALYSIS OF THE KNIFE AND SPIKE AND DROP-SPHERE TESTS.....60

4.1 Explicit Finite Element Analysis 60

4.2 Knife and Spike Model Description 61

4.3 Element types and definition 65

CHAPTER Page

4.4 Contact definition....65

4.5 Hourglass energy definition....65

4.6 Material validation....66

4.6.1 Sphere on steel plate model and results....67

4.6.2 Sphere on foam model and results....70

4.6.3 Sphere on GN2118 and AS299 model and results....72

4.7 Knife and spike resuls for Approach One Model....77

4.7.1 Knife and spike model with automatic contact definition (Approach One Model)....77

4.8 Knife model test results using Approach Two Model....81

5. CONCLUSIONS AND FUTURE WORK....86

5.1 Conclusions....86

5.2 Future Work....87

REFERENCES....88

APPENDIX

A Examples of data analysis....93

B Material damage from knife and spike testing....101

C Engineerd knife and spike....104

LIST OF TABLES

Table Page

2-1: Operating characteristic curve parameters for two factor model 13

3-1: GN 2118 Tension Test Results....42

3-2: AS299 Tension Test Results 43

3-3: Steel test results for drop-sphere test....50

3-4: Foam test results for drop-sphere test....50

3-5: GN2118 and AS299 test results for drop-sphere test 52

3-6: Energy level and corresponding heights for the drop-test set-up at ASU 54

3-7: Knife and Spike Test, Sample 1 57

3-8: Knife and Spike Test, Sample 2 57

3-9: Knife and Spike Test Results 59

4-1: Number of nodes, element type, and number of elements for each part in the knife model 64

4-2: Sensitivity analysis for a 635 mm drop of steel sphere onto steel plate 69

4-3: Experimental and FEA test results for drop-sphere test on foam....72

4-4: Approach 1 knife test calibration runs and results 81

4-5: Approach 2 knife test calibration runs and results 85

LIST OF FIGURES

Figure Page

1-1: Knife test and model components 9

3-1: Deformation zones observed in the compression test of most foams 29

3-2: GN2118 Material Morphology. (a) Fiber and shield,

(b) Fiber size and shield, (c) Cross ply, (d) Shield thickness 33

3-3: AS299 Material Morphology

(a) Weaved fabric, (b) Thickness of epoxy, (c) fiber size 35

3-4: Typical Test Setup with Fabric Sample.....40

3-5: Specimen Gripping System for GN 2118.....40

3-6: Specimen Gripping System for AS299 40

3-7: Stress/Strain Curves from GN2118 Samples 42

3-8: Stress/Strain Curves from Raw and Best Fit Data of AS299 43

3-9: Compression test set-up.....44

3-10: 25% compression on overall thickness of foam samples 46

3-11: 50% compression on the overall thickness of foam samples 46

3-12: 75% compression on the overall thickness of foam samples 47

3-13: Stress-strain curve for 25%, 50%,

and 75% sample thickness compression.....47

3-14: Drop test set-up: (a) Camera and laser level set-up

(b) testing machine and reference string.....49

3-15: GN2118 drop-test results.....51

3-16: AS299 drop-test results 52

Figure Page

3-17: Drop Test Machine and Its Components 54

3-18: (a) Height control mechanism, (b) Release mechanism 55

3-19: (a) Adhesive attached to the base plate,

(b) Adhesive attached to the backing material 56

3-20: Ready to test spike set-up 56

3-21: Sample set-up before testing with energy level 1 58

3-22: Sample after knife test 58

4-1: Knife model parts and their mesh 64

4-2: Steel sphere mesh 66

4-3: Sphere drop-test on steel plate at (a) t = 0ms and (b) t=120ms 68

4-4: Bounce height vs. time for steel plate 70

4-5: Sphere drop-test on four layers of foam at (a) t = 0 ms,

(b) t = 3 ms, and (c) t = 80 ms 71

4-6: Experimental vs. FEA results of drop-sphere test on foam 72

4-7: GN2118 Sphere drop-test on GN2118 at (a) t = 0 ms and (b) t = 3 ms, and (c)

t = 120 ms 74

4-8: Experimental vs. FEA results of drop-sphere test on GN2118 74

4-9: AS299 Sphere drop-test on GN2118 at

(a) t = 0 ms, (b) t = 3 ms, and (c) t = 103 ms 76

4-10: Experimental vs. FEA results of drop-sphere test on AS299 76

4-11: Knife and target material model at 75% penetration depth 79

4-12: Tied element in the target material 82

Figure Page

4-13: Additional nodes defined for a tied corner of four elements.....82

ABBREVATIONS

ASTM - American Society for Testing Materials

ASU – Arizona State University

FEA – Finite Element Analysis

NIJ – National Institute of Justice Standard

PMCs – Polymer Matrix composites

1. INTRODUCTION

Body armor protects humans against ballistic and stab attacks. It protects vulnerable parts of the body such as the torso and head. The design of body armor goes back to the Roman and Greek Empires when full steel armors were used. With the technological advancements in weaponry and in composite material design and manufacture, more flexible and lighter protective armors are available for use.

The type of armor used depends on the level of protection needed. For example, soldiers use ceramic based plates for the body armor because of the high threat weaponry used in battle fields. On the other hand, law-enforcement officers wear fabric based armors because they need protection against stab weaponry and hand guns.

The need for an ultra-concealable, multi-threat armor is to maximize maneuverability and conceal armor under street clothes without sacrificing the protection of law-enforcement. This type of protection is under continual investigation and much research is being done. While most ballistic threats have been stopped using aramid and ultra-high molecular weight polyethylene based materials, there is still a need in finding materials that will provide protection against stabbing threats. NIJ classifies the latter threats as those resulting from sharp weapons or knife and spike.

Filmed-resin composites have been found to work best in stopping knife and spike due to their ability to dissipate kinetic energy and restrain the movement of the weapon. The challenge is in finding the optimum number of

layers in stopping knife and spike as well as ballistic threats. The first step in optimizing the design is to develop a finite element model of the various constituents. These include the new epoxy resin composites , the knife, spike, and backing material such as foam and rubber, that are used in NIJ-certified tests. Material properties used to model these situations may be obtained experimentally or from previous research.

1.1 Literature review

Limited research data are available in the public domain dealing with stab resistant, cut resistant, and ballistic resistant materials and technology. The following review provides an understanding of flexible and protective materials such as body armor, surgical gloves, geotextiles, and impact-mitigating composites. It also provides an understanding of different modeling techniques available for these types of materials.

1.1.1 Puncture testing literature review

Body armor testing standards are developed by the Office of Law Enforcement Standards at the National Institute of Standards and Technology. The knife and spike testing standards [1] were developed in collaboration with the Police Scientific Development Branch in the United Kingdom. The research on the geometry of the standard knife and spike used for testing focused primarily with threats readily available such as knives that can be bought from retail stores. The NIJ standard also specifies minimum performance requirements and test methodology for a body-armor sample that is resistant to pointed and edged weapons.

Nguyen et al. [2] investigated the mechanisms of puncture in protective gloves, neoprene, and natural rubber using ASTM F1342 [3]. Expressions calculating the theoretical puncture force versus the varied probe geometry based on the deformation of the membrane were obtained. The authors conclude that the maximum puncture force depends on the contact surface between the material, the probe tip, the local deformation, an intrinsic material parameter, and is relatively independent of the indentor's geometry.

Erlich et al. [4] studied Zylon fabric deformation and failure during quasi-static penetration and compared the results to dynamic penetration of the same material. The deformation and failure modes present in a quasi-static test are the same as those observed in a ballistic impact. However the extent to which each mode occurs is dependent on the impact velocity and proximity to the ballistic limit. The failure modes observed are yarn pullout and yarn breakage near to and remote from the penetrator contact area. The results and analysis are used in developing a FEA material model for Zylon.

In another study, Shin et al. [5] studied the cut resistance of three high strength yarns (Zylon, Kevlar, and Spectra) under tension-shear loading conditions. This was achieved by pushing a knife blade transversely at a constant rate against a yarn gripped at its ends. The studies found that Zylon had the highest cut energy and strain to initiate cutting and Kevlar had the lowest. The studies also found that the results were a function of the slicing angle, the sharpness of the blade, and the pretension of the yarn.

Narejo and Wilson-Fahmy et al. [6] published research done in theoretical, experimental, and example studies of puncture resistance in geomembranes, a material commonly used as a liner in soil, water, or waste materials. The work includes simulation of the gravel and soil puncturing the geomembranes in the presence of hydrostatic and geostatic pressure. The geometry of the protrusion to the deformation of the geomembranes were closely studied. For a cost effective and well designed liner, the authors suggest the use of geotextiles to give an increase puncture resistance without the addition of thickness to the geomembranes.

Ghosh [7] compared failure strains for non-strained and pre-strained geotextiles, and concluded that failure strains in puncture are lower if the geotextiles are pre-strained and that further research needs to be done with testing samples biaxially.

ASTM standard F1790 [8] provides a guide to testing methods used to assess the cut resistance of a materials when exposed to a cutting edge under specified loads. The distance between the cutting edge and the material tested is measured from initial contact to cut through for each load is recorded. At least three different loadings are tested and the resulting load versus distance curve can be used to determine cut resistance of the specimen. This test method does not address puncture, tear or other modes of fabric failure. Lara et al. [9, 10, 11] did extensive research in cutting effect of degradation of blade sharpness, blade speed, sample holder type, and the load applied to the specimen. The authors also compared their work to the test methods and standards of EN 388, ASTM 1790

and ISO 13997. The authors concluded that for different sample thickness the standards did not show major errors when compared to experimental results. However, since the results depended greatly on the coefficient the results could not be compared with each other.

1.1.2 Stab Resistance Materials Literature Review

Deshmukh and McKinley [12] studied magnetorheological fluid (MRF) infused fabric that resists impact under a magnetic field. The authors found that the addition of MRF increases the absorption energy capacity. They also concluded that the energy absorbed by the MRF impregnated fabrics can be varied to satisfy specific requirements by varying the applied magnetic field and the volume fraction of MR fluid. Thermally sprayed ceramic and cement coatings on aramid fibers, such as Twaron, have been studied by Gadow et al. [13]. This type of material involves spraying heated coating onto the aramid fabric using an atmospheric plasma spray torch. The coating is cooled at the point of contact with the fabric to prevent the damage of the fibers. The coating's thickness varies between 50 to 100 μm. While the light weight and flexibility due to the thin coating of this type of material might be a better solution compared to ceramic reinforced armor, the areal density of the material is still relatively high.

Similarly, other types of materials including shear thickening fluid, which is impregnated into woven aramid fabrics, have been studied. Raghavan et al. [14, 15], Maranzano et al. [16] and Lee et al. [17] all studied rheology of the non-Newtonian fluid behavior and discussed how the increase in the viscosity of shear fluid is a key in dissipating impact energy, such as in ballistics. Studies by Lee et

al. [18,19], Wetzel et al. [20], Egres et al. [21,22] and Tan et al. [23] have shown an improved performance in ballistic mitigation performance as well as knife and spike attack of Kevlar fabric when impregnated with colloidal shear thickening fluid (STF) or polyethylene glycol (PEG). Materials treated this way are still flexible and demonstrate significant improvement in stab penetration due to an increase in the yarn pullout force. However, in order to meet NIJ requirements for knife and spike threats, these materials require a very thick armor to stop knife and spike threats, defeating the goal of a light weight, concealable armor design.

A more common material being used lately in stopping stab and ballistic threats are resin matrix composites. These materials are usually Kevlar woven materials impregnated with resin epoxy. While they are more rigid, the resin epoxy absorbs and dissipates the kinetic energy of penetration of the weapon and restrains the movement of penetration [24]. The number of layers needed to stop stab attacks and ballistic attacks is less than STF treated materials, making them ideal for light-weight, ultra-concealable armors.

1.1.3 Modeling ballistic impacts literature review

Most of work to evaluate experimental results using finite element modeling has been done in ballistic impact on fiber based materials such as Kevlar. Research by Phoenix et al. [25], Porwall et al. [26], and Taylor et al. [27] was done in investigating the wave which occurs from the impact and temperature change effect in yarn pullout. Luo et al. [28] modeled the fabric composite as a homogenous orthotropic material comprised of wavy fibers. Suresh et al. [29, 30], Giannakopoulos et al. [31] and Andrews et al. [32] focused on the analysis of

sharp objects into rate dependent metals. In this research, the equation of motion is a function of the indenter's mass are established and applying appropriate boundary conditions the maximum depth of penetration is calculated.

Work done at ASU by Sharda et al. [33] include modeling of multilayer Kevlar and Zylon fabrics used in a gas turbine engine containment system when a steel penetrator is slowly pushed through the fabric. The load deflection results are used to compute various parameters including energy absorption capacity of these materials. Similarly, Naik et al. [34], Stahlecker et al. [35], Bansal et al. [36], and Rajan et al. [37] presented work in experimental static and high strain tensile tests, shear, and friction test studies to characterize behavior of dry fabrics, such as Kevlar. A constitutive material model for this material was implemented in LS-DYNA. A comparison of FE simulations and ballistic results for a fan blade out system, used for research in fan-containment system by Federal Aviation Administration, show promising results for this constitutive model.

1.2 Thesis Objectives & Overview

1.2.1 Thesis Objectives

The major objectives of the research work are as follows:

(1) Develop the statistical procedure for determining the sample size and the veracity of experimental data from composite materials. This research culminated with development of a Graphical User Interface (GUI)-based software for reduction of experimental data.

(2) Identify body armor grade composite materials and conduct experimental tests to characterize their material properties.

(3) Develop and carry out laboratory experiments to test various armor packages that meet knife and spike threats as per NIJ standards.

(4) Study the availability of various material models in LS-DYNA for modeling the various materials used in the armor package as well as the experiments conducted in (3).

(5) Develop a sequence of LS-DYNA based finite element models to capture the experiments in (3), calibrate the models using regression analysis and experimental data, and lay the groundwork for the development of the lightest, thinnest and most comfortable, concealable armor to meet the NIJ described threats.

The knife test performed on different materials and simulated in LS-DYNA includes the following components:

(1) Drop weight attached to the knife or spike

(2) Engineered knife (Appendix C)

(3) Various configurations of composite materials

(4) Four layers of vinyl-nitrile foam

(5) Steel plate fixed at the bottom.

A sketch of the overall knife test and model is shown below in Figure 1-1.

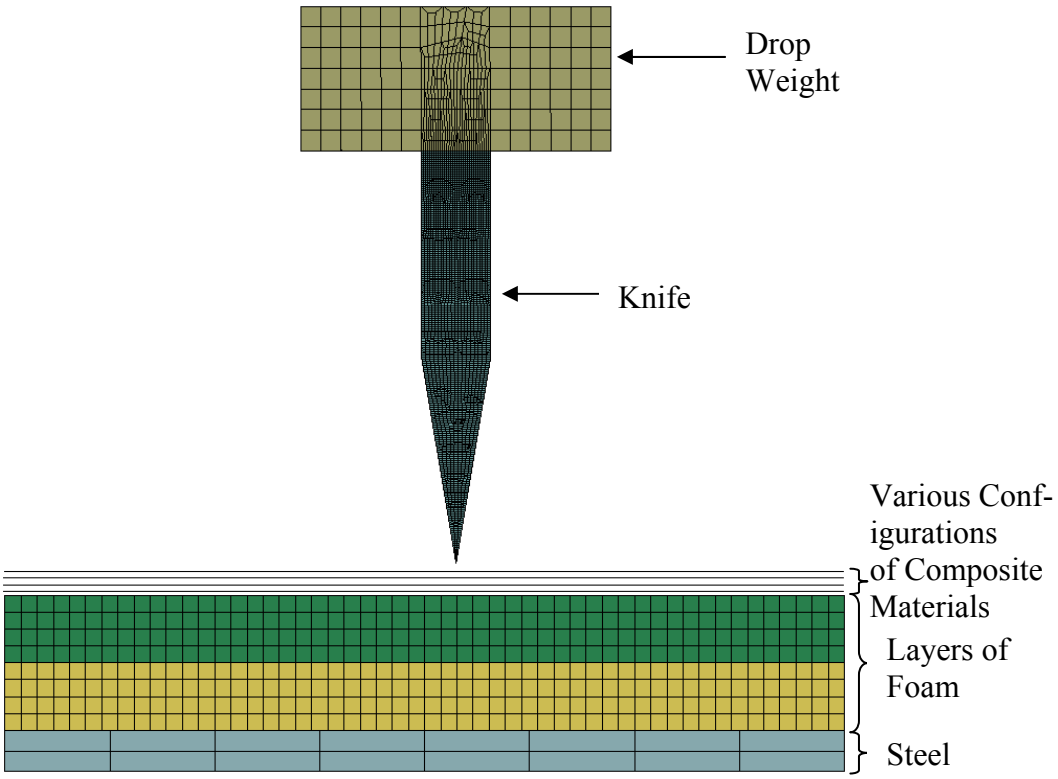

Figure 1-1: Knife test and model components

1.2.2 Thesis Overview

Design of experiments including determination of number of samples tested when running an experimental test, one and multi variable regression analysis used in predicting material properties and finite element modeling, and data smoothing techniques are discussed in Chapter 2. Experimental tests and results needed to obtain material properties for finite element modeling are presented and discussed in Chapter 3. This includes tension test for resin fiber materials, compression test for foam, drop sphere test for validating material models in LS-DYNA, and the knife and spike test used to measure maximum depth of penetration for the design of body armor. Chapter 4 discusses how the knife and spike test was built and modeled in LS-DYNA. This includes a

description of the element types used, contact definition, material models, and a comparison between FEA and experimental results for the drop-sphere test and knife and spike tests. Finally, Chapter 5 summarizes the work and includes future work that need to be done to improve the current FEA model.

2. ANALYSIS OF EXPERIMENTAL DATA

In this chapter the statistical procedure for determining the sample size, different smoothing data techniques, and regression analysis is presented. This research was used to develop a Graphical User Interface (GUI)-based software for data reduction of experimental data.

2.1 Statistical tests

When considering a set of data from which a decision needs to be drawn, null hypothesis can be used to test the hypothesis considered. These results show if the relationship between some measured phenomena has or has no affect on that decision. Null hypothesis is used in many statistical tests, including *t-test*, *F-test*. Null hypothesis is defined as follows:

$$\begin{aligned} H_0 &: \quad \beta_1 = \beta_2 = ... = \beta_k = 0 \\ H_1 &: \quad \beta_j \neq 0 \end{aligned} \tag{2.1}$$

where H_0, H_1 is the null hypothesis for a two tailed statistical test and β is some independent variable with normal distribution.

The *F-test* is a statistical test which uses null hypothesis to check if the variance of two or more samples is equal [38]. The *F-test* can either be a two-tailed test or a one-tailed test. The two-tailed version tests if the standard deviations are not equal to each other, whereas the one-tailed version only tests if the standard deviation of one population is greater or less than the second population. In multi-regression analysis, the *F-test* is used to test the quality of the fit as well as the influence of each independent variable. A general definition of the F-value in regression analysis is

$$F = \frac{SS_R / k}{SS_E / (n-k-1)} = \frac{MS_R}{MS_E} \tag{2.2}$$

where n is the number of data points, k is the degree of freedom of the model, MS_R is the mean sum of squares, and MS_E is the mean error sum of squares. A detailed description of how each variable is calculated is provided in section 2.4.3.1. Let P be the probability of seeing the observed F value if the null hypothesis is satisfied. If P is less than the confidence level α (a typical value of 0.05 is used) than H_0 is rejected.

2.2 Determination of number of samples in an experiment

The main goal for a researcher is to present information gathered from a set of samples that will best represent the population results within limits of a random error. Determining a sample size is difficult and requires collaboration of statistical analysis and desired final results. This collaboration requires either historic data from previous testing or logical estimation of the standard deviation and/or variance of the population.

If when choosing the sample size, one wants to consider the effects of a particular parameter in an experiment (e.g. cross sectional area, gage length, number of threads, etc), one can employ the operating characteristic curves. These curves plot the probability of Type II error against a parameter that reflects the extent to which the null hypothesis is false [39]. Type II error for the case of equal sample size per treatment is defined as

$$\begin{aligned} \beta &= 1 - P\{\text{Reject } H_0 \mid H_0 \text{ is false}\} \\ &= 1 - P\{F_0 > F_{\alpha, a-1, N-a} \mid H_0 \text{ is false}\} \end{aligned} \tag{2.3}$$

where the rejection of null hypothesis (H_0) is true if the probability P is less than the confidence level α.

The parameter in the operating characteristic curves that Type II error is plotted against, is defined as

$$\Phi^2 = \frac{nD^2}{2a\sigma^2} \tag{2.4}$$

where n is the number of samples, D is smallest possible value for the difference between any two conditions'(also called treatments) means, a is the total number of treatments, and σ is the standard deviation of all the treatments. The minimum Φ for which the null hypothesis would be rejected, would represent the number of samples tested.

If the sample size is needed when two parameters are taken into consideration then the minimum Φ value is calculated based on the specified difference between any treatment means. Table 2-1 below shows the definition of Φ^2 value based on the parameter of interest for which difference between treatment means is known [39]. An example of determining the sample size is shown in Appendix A.1.

Table 2-1: Operating Characteristic Curve Parameters for Two Factor Model

Parameters	Φ^2	Numerator Degrees of Freedom	Denominator Degrees of Freedom
A	$\frac{nbD^2}{2a\sigma^2}$	$a-1$	$ab(n-1)$
B	$\frac{naD^2}{2b\sigma^2}$	$b-1$	$ab(n-1)$
Interaction of AB	$\frac{nD^2}{2\sigma^2\left[(a-1)(b-1)+1\right]}$	$(a-1)(b-1)$	$ab(n-1)$

2.3 Smoothing techniques in experimental data

The primary role of experiment data is to extract information from the observed measurements. The main goal of smoothing digital raw data is to remove outliers without changing the recorded data, allowing one to perform statistical analysis on the smoothed data and to analyze the results. The two different smoothing techniques considered are moving median and moving average techniques.

2.3.1 Moving Median Smoothing Technique

Mathematically the moving median of span *N* for a set of data (x, y) can be expressed as follows

$$m_i^{[N]} = med(y_{i-u}, ..., y_i, ..., y_{i+u}) \tag{2.5}$$

where *i* is 1 to *n*, with *n* being the size of the data set, $u = \frac{N-1}{2}$, N is number of points (span size) that the filter will process data at a time, $m_i^{[N]}$ is the new value of y at *i,* and median is the middle observation in rank order of *y* [40]. The end values for this process are kept the same and depending on the need, the data can be smoothed multiple times.

2.3.2 Moving Average Filters

There are two types of moving average filters

- Simple moving average
- Polynomial moving average

These above mentioned methods smooth the data by fitting a type of predetermined function to an odd amount of points from the data, calculating a

weighted or non-weighted average of the points at the center abscissa of the group, dropping the last point at one end of the group, and repeating the process so as to obtain a smoother data. If Y_j^s represents the data points, then the smoothing process is implemented as follows

$$Y_j^s = \frac{\sum_{i=-m}^{i=m} C_i Y_{j+i}}{N} \tag{2.6}$$

where C_i is the scaling factor, N is the sum of the scaling factors C_i, and j is the running index of the ordinate data and *m* is the number of points used to run the smoothing process at each point [41].

In the case of the simple moving average, a line is fitted using a predetermined number of points. In this case C_i is equal to 1 and N is the number of points used to for smoothing. Polynomial moving average is a type of weighted moving average which is derived from the least square curve fitting method. The value of C_i that appears in equation (2.6) is a function of the number of points and the type of polynomial used to best fit the data.

2.4 Regression analysis

Data analysis frequently involves fitting a mathematical model to a set of experimental data. One of the most common and simple methods used to get a mathematical model is linear regression. This method creates a model with a linear relationship between the dependent and independent variable. Linear regression can involve one-variable or multiple variable models.

2.4.1 One-variable regression analysis

2.4.1.1 Linear and Polynomial Fitting

The general equation for k^{th} degree polynomial is

$$\hat{y} = a_0 + a_1 x + ... + a_k x^k \tag{2.7}$$

The error between the raw and regression fit data, also known as regression value, can be calculated using the least squares method

$$R^2 = \sum_{i=1}^{n} \left[y_i - \left(a_0 + a_1 x_i + ... + a_k x_i^{\,k} \right) \right]^2 \tag{2.8}$$

R-squared would be zero if a set of data would fit a k^{th} order polynomial perfectly. In order to get the best possible fit, one can try and minimize the value of R-squared. This can be achieved by finding the values of $a_0, a_1, ..., a_k$ that minimize the residual [42]. So, taking the derivative of R-squared with respect to $a_0, a_1, ..., a_k$ it is seen that

$$\begin{aligned}
&\frac{\partial (R^2)}{\partial a_0} = -2 \sum_{i=1}^{n} \left[y_i - \left(a_0 + a_1 x_i + ... + a_k x_i^{\,k} \right) \right] = 0 \\
&\frac{\partial (R^2)}{\partial a_1} = -2 \sum_{i=1}^{n} \left[y_i - \left(a_0 + a_1 x_i + ... + a_k x_i^{\,k} \right) \right] x_i = 0 \\
&\vdots \\
&\frac{\partial (R^2)}{\partial a_k} = -2 \sum_{i=1}^{n} \left[y_i - \left(a_0 + a_1 x_i + ... + a_k x_i^{\,k} \right) \right] x_i^{\,k} = 0
\end{aligned} \tag{2.9}$$

Distributing the summation sign to equation (2.9):

$$\begin{aligned}
&\sum_{i=1}^{n} y_i - na_0 - a_1\sum_{i=1}^{n} x_i - \ldots - a_k\sum_{i=1}^{n} x_i^{\,k} = 0\\
&\sum_{i=1}^{n} x_i y_i - a_0\sum_{i=1}^{n} x_i - a_1\sum_{i=1}^{n} x_i^{\,2} - \ldots - a_k\sum_{i=1}^{n} x_i^{\,k+1} = 0\\
&\vdots\\
&\sum_{i=1}^{n} x_i^{\,k} y_i - a_0\sum_{i=1}^{n} x_i^{\,k} - a_1\sum_{i=1}^{n} x_i^{\,k+1} - \ldots - a_k\sum_{i=1}^{n} x_i^{\,2k} = 0
\end{aligned} \tag{2.10}$$

Grouping similar terms in equation (2.10)

$$\begin{aligned}
&\sum_{i=1}^{n} y_i = na_0 + a_1\sum_{i=1}^{n} x_i + \ldots + a_k\sum_{i=1}^{n} x_i^{\,k}\\
&\sum_{i=1}^{n} x_i y_i = a_0\sum_{i=1}^{n} x_i + a_1\sum_{i=1}^{n} x_i^{\,2} + \ldots + a_k\sum_{i=1}^{n} x_i^{\,k+1}\\
&\vdots\\
&\sum_{i=1}^{n} x_i^{\,k} y_i = a_0\sum_{i=1}^{n} x_i^{\,k} + a_1\sum_{i=1}^{n} x_i^{\,k+1} + \ldots + a_k\sum_{i=1}^{n} x_i^{\,2k}
\end{aligned} \tag{2.11}$$

Or in matrix notation

$$\begin{bmatrix}
n & \sum_{i=1`}^{n} x_i & \cdots & \sum_{i=1`}^{n} x_i^{\,k}\\
\sum_{i=1`}^{n} x_i & \sum_{i=1`}^{n} x_i^{\,2} & \cdots & \sum_{i=1`}^{n} x_i^{\,k+1}\\
\vdots & \vdots & \ddots & \vdots\\
\sum_{i=1`}^{n} x_i^{\,k} & \sum_{i=1`}^{n} x_i^{\,1+k} & \cdots & \sum_{i=1`}^{n} x_i^{\,2k}
\end{bmatrix}
\begin{bmatrix} a_0\\ a_1\\ \vdots\\ a_k \end{bmatrix} =
\begin{bmatrix} \sum_{i=1}^{n} y_i\\ \sum_{i=1`}^{n} x_i y_i\\ \vdots\\ \sum_{i=1`}^{n} x_i^{\,k} y_i \end{bmatrix} \tag{2.12}$$

The above matrix is a Vandermonde matrix. So the solution to the polynomial coefficients can be written as follows

$$\begin{bmatrix}
1 & x_1 & x_1^{\,2} & \cdots & x_1^{\,k}\\
1 & x_2 & x_2^{\,2} & \cdots & x_2^{\,k}\\
\vdots & \vdots & \vdots & \ddots & \vdots\\
1 & x_n & x_n^{\,2} & \cdots & x_n^{\,k}
\end{bmatrix}
\begin{bmatrix} a_0\\ a_1\\ \vdots\\ a_k \end{bmatrix} =
\begin{bmatrix} y_1\\ y_2\\ \vdots\\ y_n \end{bmatrix} \tag{2.13}$$

or,

$$\mathbf{y} = \mathbf{X}\mathbf{a} \tag{2.14}$$

To show equation (2.14) is true, multiply both sides of the above equation with $\mathbf{X}^{\mathbf{T}}$

$$\begin{bmatrix} 1 & 1 & \cdots & 1 \\ x_1 & x_2 & \cdots & x_n \\ x_1^{\,2} & x_2^{\,2} & \cdots & x_n^{\,2} \\ \vdots & \vdots & \ddots & \vdots \\ x_1^{\,k} & x_2^{\,k} & \cdots & x_n^{\,k} \end{bmatrix} \begin{bmatrix} 1 & x_1 & x_1^{\,2} & \cdots & x_1^{\,k} \\ 1 & x_2 & x_2^{\,2} & \cdots & x_2^{\,k} \\ \vdots & \vdots & \vdots & \ddots & \vdots \\ 1 & x_n & x_n^{\,2} & \cdots & x_n^{\,k} \end{bmatrix} \begin{bmatrix} a_0 \\ a_1 \\ \vdots \\ a_k \end{bmatrix} =$$

$$\begin{bmatrix} 1 & 1 & \cdots & 1 \\ x_1 & x_2 & \cdots & x_n \\ x_1^{\,2} & x_2^{\,2} & \cdots & x_n^{\,2} \\ \vdots & \vdots & \ddots & \vdots \\ x_1^{\,k} & x_2^{\,k} & \cdots & x_n^{\,k} \end{bmatrix} \begin{bmatrix} y_1 \\ y_2 \\ \vdots \\ y_n \end{bmatrix} \rightarrow \begin{bmatrix} n & \sum_{i=1`}^{n} x_i & \cdots & \sum_{i=1`}^{n} x_i^{\,k} \\ \sum_{i=1`}^{n} x_i & \sum_{i=1`}^{n} x_i^{\,2} & \cdots & \sum_{i=1`}^{n} x_i^{\,k+1} \\ \vdots & \vdots & \ddots & \vdots \\ \sum_{i=1`}^{n} x_i^{\,k} & \sum_{i=1`}^{n} x_i^{\,1+k} & \cdots & \sum_{i=1`}^{n} x_i^{\,2k} \end{bmatrix} \begin{bmatrix} a_0 \\ a_1 \\ \vdots \\ a_k \end{bmatrix} =$$

$$\begin{bmatrix} \sum_{i=1}^{n} y_i \\ \sum_{i=1`}^{n} x_i y_i \\ \vdots \\ \sum_{i=1`}^{n} x_i^{\,k} y_i \end{bmatrix} \tag{2.15}$$

Hence, the solution to the *a* coefficients is

$$\mathbf{a} = (\mathbf{X}^{\mathbf{T}}\mathbf{X})^{-1}\mathbf{X}^{\mathbf{T}}\mathbf{y} \tag{2.16}$$

Equations (2.2) to (2.5) are applicable for a linear fit or straight line fit also. In matrix notation the linear fit can be expressed as

$$\begin{bmatrix} 1 & x_1 \\ 1 & x_2 \\ \vdots & \vdots \\ 1 & x_n \end{bmatrix} \begin{bmatrix} a_0 \\ a_1 \end{bmatrix} = \begin{bmatrix} y_1 \\ y_2 \\ \vdots \\ y_n \end{bmatrix} \tag{2.17}$$

2.4.1.2 Exponential fitting

The general formula for the exponential best fit function is

$$y = Ae^{Bx} \tag{2.18}$$

In order to find the values of A and B, the above formula is linearized so that the linear least square method can be used to solve for the A and B coefficients. This is achieved by taking the natural log of equation (2.6).

$$\ln y = \ln Ae^{Bx} = \ln A + \ln e^{Bx} = \ln A + Bx \tag{2.19}$$

Following the same theory as in 2.4.1.1 one can solve for *A* and *B* as follows

$$\begin{bmatrix} 1 & x_1 \\ 1 & x_2 \\ \vdots & \vdots \\ 1 & x_n \end{bmatrix} \begin{bmatrix} a_0 \\ a_1 \end{bmatrix} = \begin{bmatrix} \ln y_1 \\ \ln y_2 \\ \vdots \\ \ln y_n \end{bmatrix} \tag{2.20}$$

In matrix notation

$$\mathbf{a} = (\mathbf{X}^{\mathbf{T}}\mathbf{X})^{-1}\mathbf{X}^{\mathbf{T}} \ln \mathbf{y} \tag{2.21}$$

where

$$A = \exp(a_0) \tag{2.22}$$

$$B = a_1 \tag{2.23}$$

2.4.1.3 Logarithmic fitting

The general formula for a logarithmic fit is

$$y = A + B \ln x \tag{2.24}$$

Since equation (2.24) is in a similar form as a linear function $y = A + Bx$. The equations for logarithmic fitting can be written as

$$\begin{bmatrix} 1 & \ln x_1 \\ 1 & \ln x_2 \\ \vdots & \vdots \\ 1 & \ln x_n \end{bmatrix} \begin{bmatrix} a_0 \\ a_1 \end{bmatrix} = \begin{bmatrix} y_1 \\ y_2 \\ \vdots \\ y_n \end{bmatrix} \tag{2.25}$$

In matrix notation

$$\mathbf{a} = (\mathbf{X}^\mathbf{T}\mathbf{X})^{-1}\mathbf{X}^\mathbf{T}\mathbf{y} \tag{2.26}$$

For

$$\mathbf{X} = \begin{bmatrix} 1 & \ln x_1 \\ 1 & \ln x_2 \\ \vdots & \vdots \\ 1 & \ln x_n \end{bmatrix}, \ \mathbf{y} = \begin{bmatrix} y_1 \\ y_2 \\ \vdots \\ y_n \end{bmatrix} \tag{2.27}$$

and

$$A = a_0 \tag{2.28}$$

$$B = a_1 \tag{2.29}$$

2.4.2 Correlation Coefficient

The correlation coefficient also known as cross-correlation factor is a value that describes the quality of a fit for a set of data. In linear regression the value of R^2 is a between 0 and 1 and is unitless. When R^2 equals 0 it means that the curve does not fit the data better than a horizontal line going through the mean of the data would. When R^2 equals 1, it means that the all points lie on the curve and there is no scatter.

R^2 is calculated from the sum of squares of the vertical distance of the points from the best-fit curve, SS_{reg}, and the sum of squares of the vertical distance of the points from a horizontal line through the mean of all Y values, SS_{tot} [43]. The equations for SS_{reg}, SS_{tot}, and R^2 are

$$SS_{reg} = \sum_{i=1}^{n} (y_i - \hat{y})^2 \tag{2.30}$$

$$SS_{tot} = \sum_{i=1}^{n} (y_i - \bar{y})^2 \tag{2.31}$$

$$R^2 = 1 - \frac{SS_{reg}}{SS_{tot}} \tag{2.32}$$

where $\hat{y}_i$ are the y_i values corresponding to the best fit curve and the raw data, respectively. The mean value $\bar{y}$, for the given raw set of data can be computed as

$$\bar{y} = \frac{\sum_{i=1}^{n} y_i}{n} \tag{2.33}$$

2.4.3 Multi-variable regression analysis

The relationship between a dependent variable y and two or more independent variables $x_1, x_2, \ldots, x_n$ is determined by a regression model called multiple-regression analysis. A first order multiple-regression model [39] with k independent variables and N number of data points, takes the form of:

$$y = a_0 + \sum_{j=1}^{k} a_j x_j + \sum\sum_{i<j} a_{ij} x_i x_j + \varepsilon \tag{2.34}$$

or in matrix notation:

$$\mathbf{y = Xa + e} \tag{2.35}$$

where

- y_i is the observational data
- a_j are the regression coefficients
- x_i are the predictor variables
- i represents the ith data point
- k is the number of design variables.
- ε is the statistical/experimental error

The regression coefficients above can be found by applying the method of least squares. Through this method the values of vector **a** are computed such that the square of the errors, ε_i, are minimized. The least square function is defined as

$$L = \sum_{i=1}^{n} \varepsilon_i^{\,2} = \sum_{i=1}^{n} \left(y_i - a_0 - \sum_{j=1}^{k} a_j x_j - \sum_{i=1}^{k} \sum_{j=1}^{k} a_{ij} x_i x_j \right)^2 \tag{2.36}$$

Minimizing equation (2.36) with respect to $a_0, a_1, ..., a_5$

$$\begin{aligned}
&\frac{\partial L}{\partial a_0} = -2 \sum_{i=1}^{n} \left(y_i - a_0 - \sum_{j=1}^{k} a_j x_j - \sum_{i=1}^{k} a_{ii} x_i^{\,2} - \sum_{i=1}^{k} \sum_{j=1}^{k} a_{ij} x_i x_j \right) = 0 \\
&\left. \frac{\partial L}{\partial a_j} \right|_{j=1,2,..,k} = -2 \sum_{i=1}^{n} \left(y_i - y_i - a_0 - \sum_{j=1}^{k} a_j x_j - \sum_{i=1}^{k} \sum_{j=1}^{k} a_{ij} x_i x_j \right) x_j = 0 \\
&\left. \frac{\partial L}{\partial a_{ij}} \right|_{i=1,2,..,k,\, j=1,2,..,k} = \\
&-2 \sum_{i=1}^{n} \left(y_i - y_i - a_0 - \sum_{j=1}^{k} a_j x_j - \sum_{i=1}^{k} a_{ii} x_i^{\,2} - \sum_{i=1}^{k} \sum_{j=1}^{k} a_{ij} x_i x_j \right) x_i x_j = 0
\end{aligned} \tag{2.37}$$

A first order, two variable multiple-regression equation can be written as follows

$$y_i = a_0 + a_1 x_1 + a_2 x_2 + a_3 x_1 x_2 + \varepsilon_i \tag{2.38}$$

Distributing the summation sign for the first order, two independent variable regression equation and simplifying we obtain

$$\begin{bmatrix} n & \sum_{i=1}^{n} x_{i1} & \sum_{i=1}^{n} x_{i2} & \sum_{i=1}^{n} x_{i1}x_{i2} \\ \sum_{i=1}^{n} x_{i1} & \sum_{i=1}^{n} x_{i1}^{\,2} & \sum_{i=1}^{n} x_{i1}x_{i2} & \sum_{i=1}^{n} x_{i1}^{\,2}x_{i2} \\ \sum_{i=1}^{n} x_{i2} & \sum_{i=1}^{n} x_{i1}x_{i2} & \sum_{i=1}^{n} x_{i2}^{\,2} & \sum_{i=1}^{n} x_{i1}x_{i2}^{\,2} \\ \sum_{i=1}^{n} x_{i1}x_{i2} & \sum_{i=1}^{n} x_{i1}^{\,2}x_{i2} & \sum_{i=1}^{n} x_{i1}x_{i2}^{\,2} & \sum_{i=1}^{n} x_{i1}^{\,2}x_{i2}^{\,2} \\ \sum_{i=1}^{n} x_{i1}^{\,2} & \sum_{i=1}^{n} x_{i1}^{\,3} & \sum_{i=1}^{n} x_{i1}^{\,2}x_{i2} & \sum_{i=1}^{n} x_{i1}^{\,3}x_{i2} \\ \sum_{i=1}^{n} x_{i2}^{\,2} & \sum_{i=1}^{n} x_{i1}x_{i2}^{\,2} & \sum_{i=1}^{n} x_{i2}^{\,3} & \sum_{i=1}^{n} x_{i1}x_{i2}^{\,3} \end{bmatrix} \begin{bmatrix} a_0 \\ a_1 \\ a_2 \\ a_3 \end{bmatrix} = \begin{bmatrix} \sum_{i=1}^{n} y_i \\ \sum_{i=1}^{n} y_i x_{i1} \\ \sum_{i=1}^{n} y_i x_{i2} \\ \sum_{i=1}^{n} y_i x_{i1} x_{i2} \end{bmatrix} \tag{2.39}$$

The above matrix is a Vandermonde matrix. Simplifying the above expression lets us write the solution to the first order multiple-regression as follows

$$\begin{bmatrix} 1 & x_{11} & x_{12} & x_{11}x_{12} \\ 1 & x_{21} & x_{22} & x_{21}x_{22} \\ \vdots & \vdots & \vdots & \vdots \\ 1 & x_{n1} & x_{n2} & x_{n1}x_{n2} \end{bmatrix} \begin{bmatrix} a_0 \\ a_1 \\ a_2 \\ a_3 \end{bmatrix} = \begin{bmatrix} y_1 \\ y_2 \\ \vdots \\ y_n \end{bmatrix} \tag{2.40}$$

2.4.3.1 Goodness of fit

One of the parameters to check the goodness of fit in a multi-regression problem is the coefficient of multiple determination, R^2, defined as

$$R^2 = 1 - \frac{SS_E}{SS_T} \tag{2.41}$$

R^2, however, can increase as more variables are added to the model; hence an adjusted coefficient is required to prevent this increase. Equation (2.42) below shows an equation for the adjusted coefficient.

$$R_{adj}{}^2 = 1 - \frac{SS_E/(n-p)}{SS_T/(n-1)} = 1 - \frac{n-1}{n-p}\left(1-R^2\right) \tag{2.42}$$

In order to check if the regression model is a good indication of the true situation, the one one-tailed *F*-test is used. As described in section 2.1 this method tests the hypothesis that the regression is not significant by calculating an *F* value based on the sum of squares, the degree of freedom, and the number of points.

$$SS_T = SS_R + SS_E \tag{2.43}$$

$$SS_R = \mathbf{a'X'y} - \frac{\left(\sum_{i=1}^{n} y_i\right)^2}{n} \tag{2.44}$$

$$SS_E = \mathbf{y'y - a'X'y} \tag{2.45}$$

where

- SS_R is the regression sum of squares
- SS_E is the error sum of squares
- **a** is the vector storing polynomial coefficients
- **X** is the matrix containing the independent variable data
- **y** is the matrix containing the dependent variable values

The statistic F_0 is calculated as

$$F_0 = \frac{SS_R/k}{SS_E/(n-k-1)} = \frac{MS_R}{MS_E} \tag{2.46}$$

where

- n is the number of data points
- k is the degree of freedom of the model
- MS_R is the mean sum of squares
- MS_E is the mean error sum of squares.

H_0 is rejected if the probability of seeing the observed F_0 value is less than the confidence level α (a typical value of 0.05 is used). Rejection of H_0 implies that at least one of the independent variables contributes significantly to the model. This can help the scientist decide if some of the independent variables in the model are unnecessary.

To see the influence value of the individual variables on the model equation, partial *F-tests* on individual and group of coefficients can be performed. In this case, the regression sum of squares due to a coefficient of regression is written as $SS_R(a)$ (where a is one of the regression coefficients in the model). To find the contribution of each individual term, the null hypothesis is assumed to be true ($H_0 : a_j = 0$). To better understand this process, let us look at a linear, two variable model

$$y = X_1 a_1 + X_2 a_2 \tag{2.47}$$

If we look at the contribution of a_1, the regression sum of squares is

$$SS_R(a_2) = \mathbf{a_2 X'_2 y} \tag{2.48}$$

If we define the sum of squares due to a_1 given that a_2 is already in the model, the regression sum of squares can be written as:

$$SS_R\left(a_1 \mid a_2\right) = SS_R - SS_R\left(a_2\right) \tag{2.49}$$

The partial *F-test* is than defined as

$$F_0 = \frac{SS_R\left(a_1 \mid a_2\right)/k}{MS_E} \tag{2.50}$$

where

- k is the degree of freedom of the regression model
- MS_E is the mean error sum of squares for the entire regression model.

Similar to the *F-test* for the entire regression model, H_0 is rejected if the probability of seeing the observed F_0 for the individual or group variables is less than the confidence level α (a typical value of 0.05 is used). Rejection of H_0 implies that for equation (2.47) the independent variable, X_1, contributes significantly to the regression model.

3. MATERIAL MODEL DESCRIPTIONS AND EXPERIMENTAL TESTS

There are four different materials used in the knife and spike experimental test and model. The supporting materials used during testing are steel and vinyl-nitrile foam. The materials used to model and test armor protection are Kevlar-based composite identified as AS299, AS400, and GN2118. In this chapter, each of these materials are defined and characterized. Also, available LS-DYNA models are evaluated and the most suitable model is chosen. Finally experimental tests, needed to obtain material properties for each of these materials, and their results are presented. These tests include uniaxial-tensile test for the composite materials and compression test for the vinyl-nitrile foam. A drop-sphere test was also done to validate the material models chosen for an impact test. Finally the knife and spike experimental results are presented in this chapter.

3.1 Material Descriptions

3.1.1 Steel Material

The steel material specified for the engineered knife and spike by NIJ is Ground Flat Stock O-1 Harden and Temper 52-55 Rockwell C. This a low-alloy cold-work tool steel with a low tendency to shrinking and warping. Its main use is in cutting tools, such as knives [44].

3.1.2 Steel Material Models in LS-DYNA

Three different material models were considered for steel:

- *MAT_PLASTIC_KINEMATIC – this material is suited to model isotropic materials with the option of including rate effects.
- *MAT_ELASTIC – this material is suited for elastic material models.

- *MAT_RIGID – this is a rigid body material. Material properties such as modulus of elasticity, density, and Poisson's ratio are specified, however, for determining sliding interface parameters when rigid body is in contact with other parts.

Since damages to the knife during experimental testing are observed to be very minimal and all the other steel parts are not subjected to any damage, all steel parts are modeled as rigid materials. The rigid material model was also used to avoid instabilities due to knife element erosions when contact between knife and target material is initiated. The material properties needed for this material definition are as follows:

- Density
- Modulus of elasticity
- Poisson's ratio

Since steel is a common material with well tested and proved material property values, no experimental testing was performed for this material.

3.1.3 Foam material

Available foam used as a backing material is vinyl-nitrile foam. This is a closed-cell impact absorbing foam.

3.1.2 Foam Material Models in LS-DYNA

There are many material models available in LS-DYNA for rubber, foam, and other highly compressible materials. Based on the work by Croop et al. [45] on the selecting material models when simulating foams in LS-DYNA, the authors focus on compression as a mode of deformation. When foam is subjected

to a compressive test, there are three zones in the compressive stress-strain relationship that are observed as shown below in Figure 3-1. Zone 1 represents the initial region when the foam shows stiffness due to the strength of the foam. Zone 2 represents a flatter region when the gas inside the foam is compressed. Zone 3 represents the densification of the foam (foam cell collapse), in which case the stress-strain curve is steep.

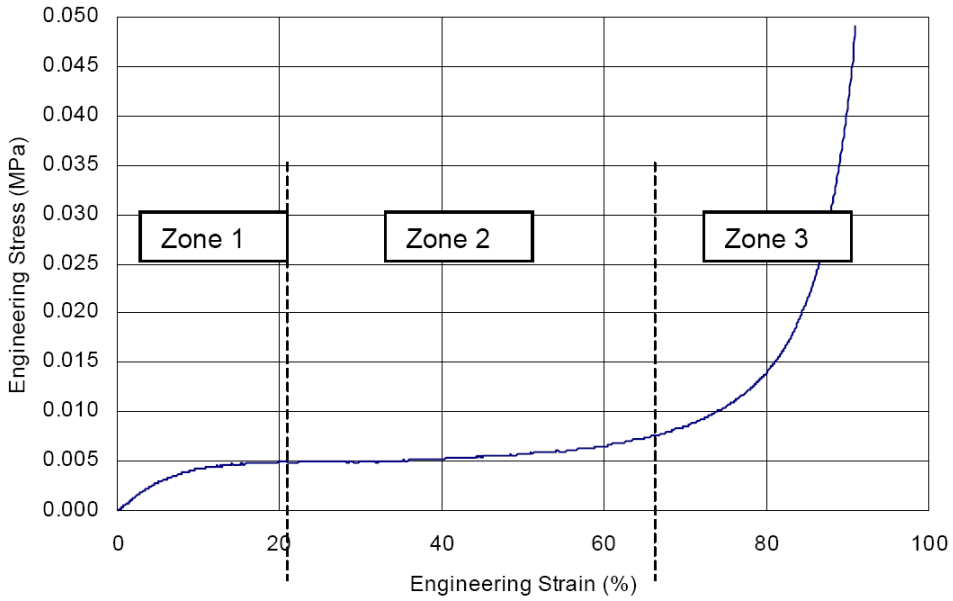

Figure 3-1: Deformation zones observed in the compression test of most foams [45]

The material models available for this mode of deformation evaluated for this research work are:

- MAT_ LOW_DENSITY_FOAM (MAT_57) – this model is used in modeling highly compressible density foams.
- MAT_CRUSHABLE_FOAM (MAT_63) - this material is used to model crushable foams.

- MAT_FU_CHANG_FOAM (MAT_83) – this foam model includes rate effects in low and medium density foams.
- MAT_MODIFIED_CRUSHABLE_FOAM (MAT_163) – this model is used in modeling crushable foams with rate effects.
- MAT_LOW_DENSITY_SYNTHETIC_FOAM (MAT_179) – this is an improved version of MAT_57, may includes failure criteria and orthotropic behavior of foam.

From the compression test results presented in section 3.4.5 it is apparent that the foam used as a backing material in the knife and spike test has all three zones in the stress strain curve. Because unloading data is not important for the knife and target material model, the most suitable material model for this particular foam is MAT_LOW_DENSITY_FOAM. This type of foam is used to model highly compressible foam with option of energy dissipation factor and hysteresis of unloading to be specified. For this model it is assumed that in tension material behaves in a linear fashion until tearing occurs [53]. This model also uses compression nominal stress versus strain data for the loading curve, which for the vinyl-nitrile foam used in modeling the backing material, this curve is obtained from the foam compression test.

3.1.5 Dry fabrics material

The two fabrics tested and presented are GN2118 and AS299. The main purpose of GN2118 is to protect against ballistic threats, while AS299 is used to protect against stab threats.

Both these materials are polymer matrix composites containing aramid fibers. While information on the fabrication of these materials is not in public domain, GN2118 is a Honeywell product consisting of two plies of unidirectional Kevlar fiber, cross-plied at zero degrees and 90 degrees. The material is light (areal density is 110 g/m^2) and has strong resistance to environmental exposure [46]. AS299 is Kevlar fabric with epoxy resin injected into the fabric and is manufactured by SAATI Protection and Composites, Italy.

High electron resolution microscopy (SEM microscopy) was used to analyze the morphology of these materials. ¼in specimens were prepared and gold coated to prevent specimen charging when placed in the SEM microscope. Images obtained from this analysis of the two materials are shown below in Figure 3-2 and Figure 3-3. The images show that fiber size is similar for both materials at approximately 12 μm. However GN2118 has a much thinner shield than the epoxy on AS299. From the figures below it can also be observed that GN2118 delaminates while AS299 is held together very tightly by the epoxy present.

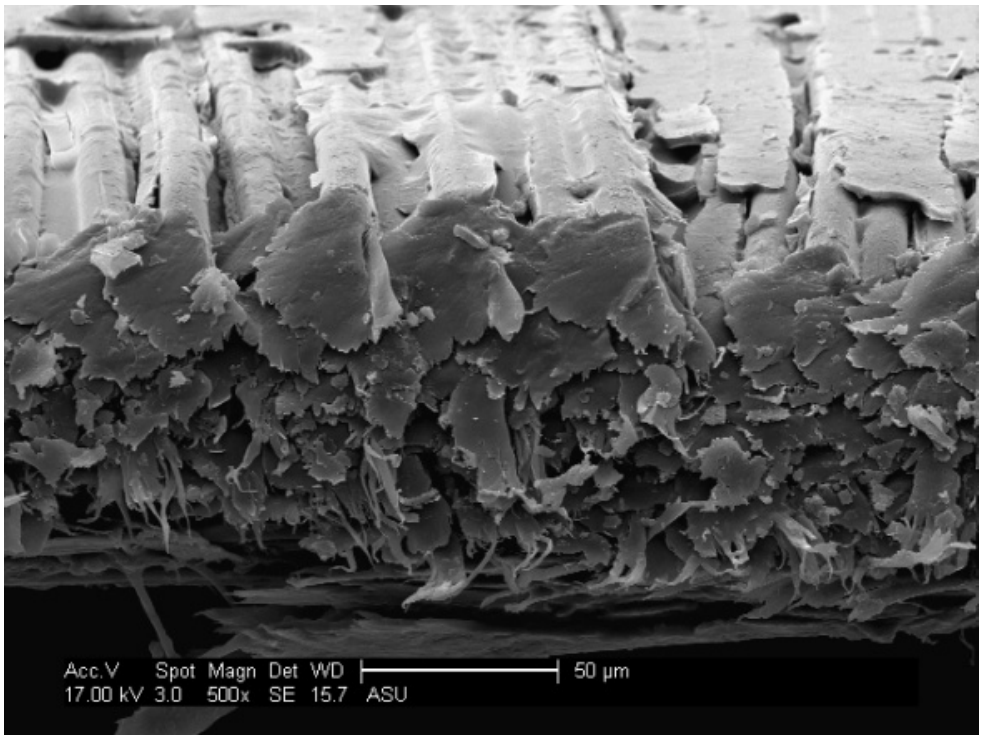
Acc.V Spot Magn Det WD 50 µm
17.00 kV 3.0 500x SE 15.7 ASU

(a)

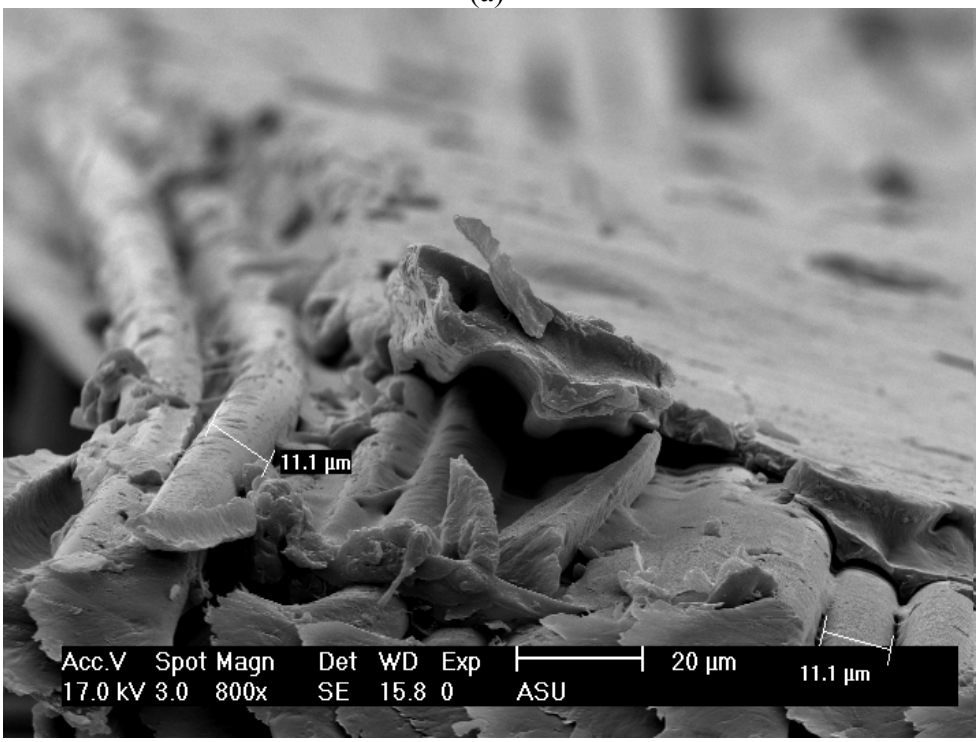
11.1 µm
Acc.V Spot Magn Det WD Exp 20 µm
17.0 kV 3.0 800x SE 15.8 0 ASU
11.1 µm

(b)

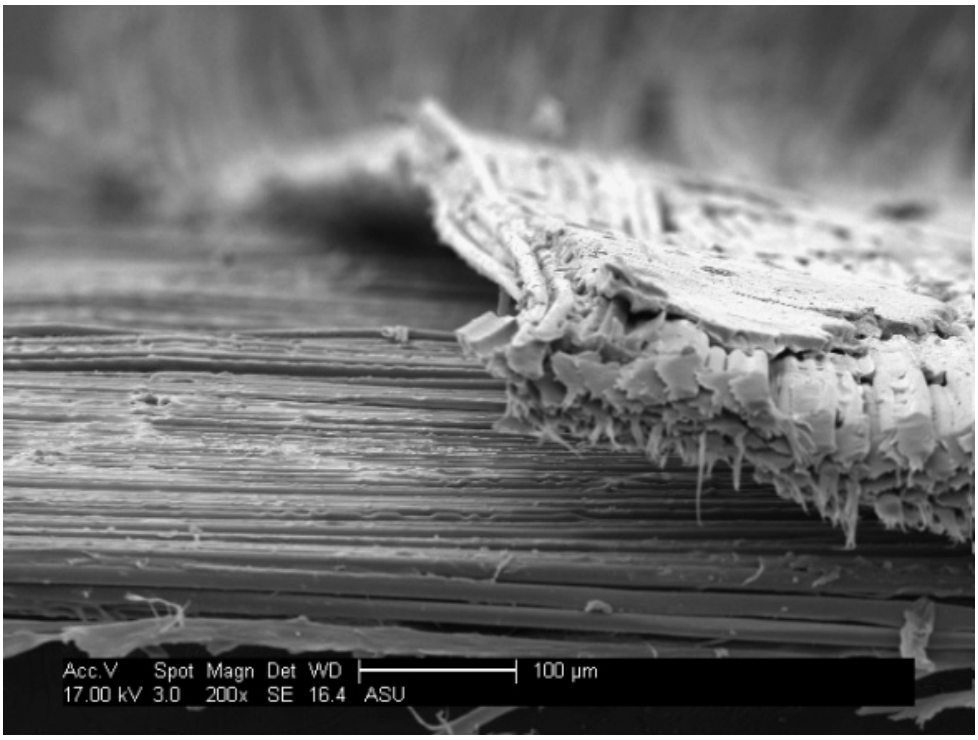

(c)

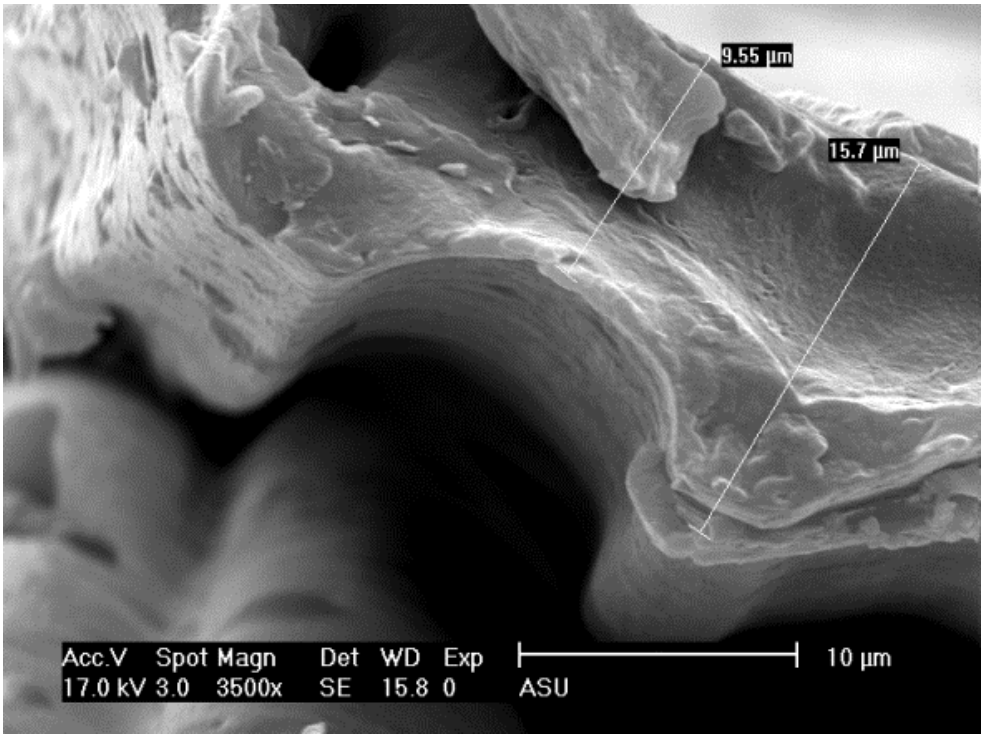

(d)

Figure 3-2: GN2118 Material Morphology. (a) Fiber and shield, (b) Fiber size and shield, (c) Cross ply, (d) Shield thickness

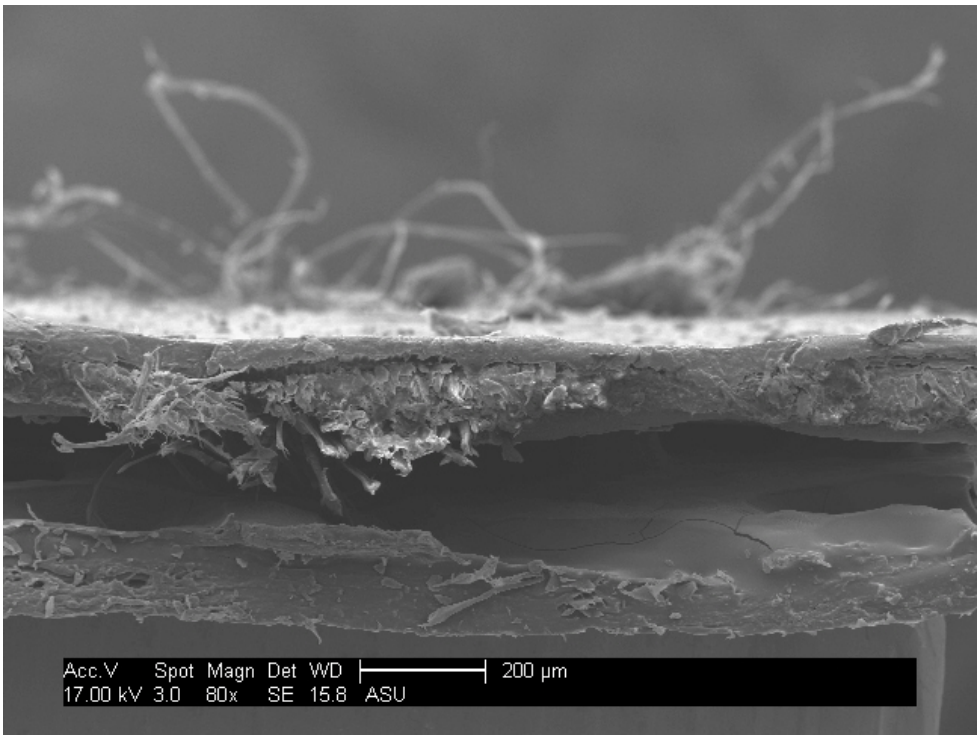
Acc.V Spot Magn Det WD 200 µm
17.00 kV 3.0 80x SE 15.8 ASU

(a)

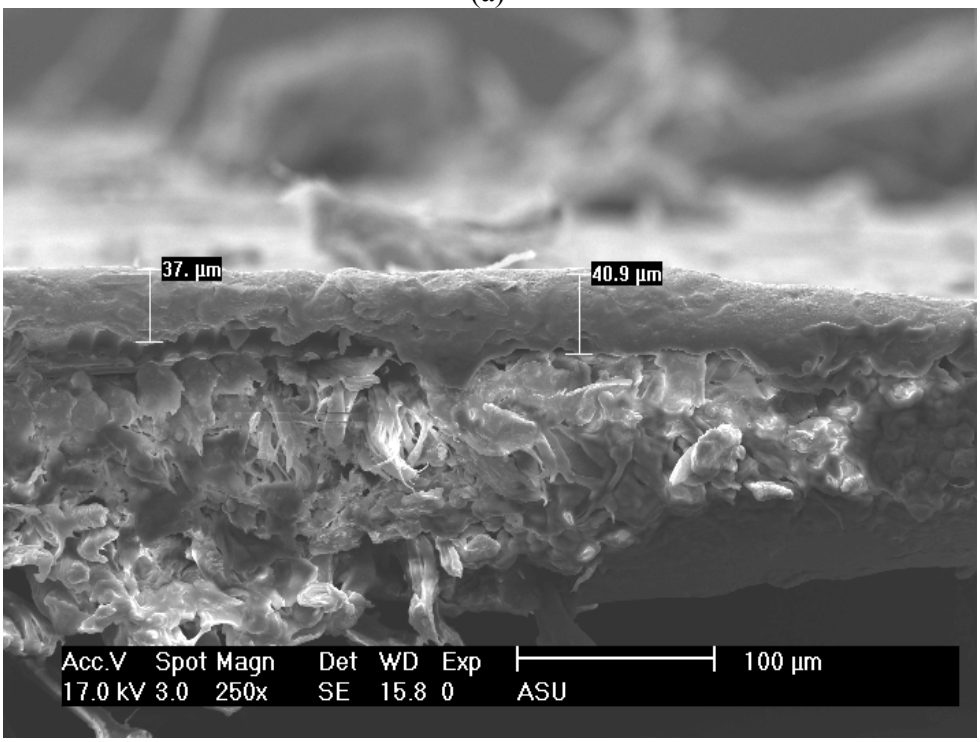
37. µm
40.9 µm
Acc.V Spot Magn Det WD Exp 100 µm
17.0 kV 3.0 250x SE 15.8 0 ASU

(b)

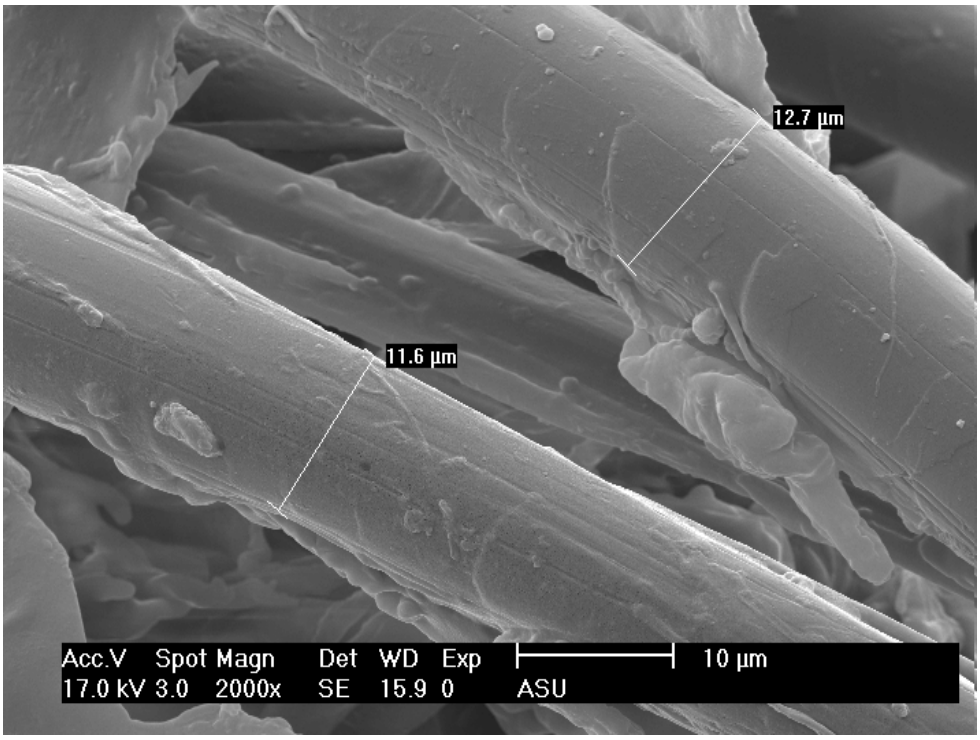

(c)

Figure 3-3: AS299 Material Morphology. (a) Weaved fabric, (b) Thickness of epoxy, (c) fiber size

3.1.6 Composite material models considered in LS-DYNA

Several material models were considered when modeling GN2118 and AS299. A list of these materials and a brief description are given below.

- MAT_COMPOSITE_DAMAGE (MAT_22) – composite material model with no rate sensitivity
- MAT_ENHANCED_COMPOSITE_DAMAGE CHANG_FAILURE (MAT_54) – enhanced version of MAT-022, with strain failure criteria for shear, compression, and tension
- MAT_ENHANCED_COMPOSITE_DAMAGE TSAI-WU FAILURE (MAT_55) – similar to MAT_54, but with Tsai-Wu failure criteria.

- MAT_LAMINATED_COMPOSITE_FABRIC (MAT_58) - Similar to the previous material models with no rate sensitivity but with more material property parameters.
- MAT_COMPOSITE_FAILURE_MODEL (MAT_59) No rate sensitivity; solids and shells
- MAT_COMPOSITE_LAYUP (MAT_116) - This is an elastic model with no damage or failure and works for shell elements only
- MAT_COMPOSITE_MATRIX (MAT_117) – similar to MAT_116
- MAT_COMPOSITE_DIRECT (MAT_118) – similar to MAT_116
- MAT_RATE_SENSITIVE_COMPOSITE_FABRIC (MAT_158) - Matzenmiller with rate sensitivity added using viscous stress tensor; shell only
- MAT_COMPOSITE_MSC (MAT_161/162) – this model has rate sensitivity and it is applicable for shells and solids

MAT_22 was chosen to model these materials since the experimental characterization of the two materials was limited to tensile testing only. Considering that GN2118 and AS299 are very thin composite materials, only in-plane properties are considered. Chang-Chang Composite Failure material model used to model AS299 and GN2118 is based on orthotropic material model. This type of model will consider only the in-plane properties of the materials defined. The parameters required for this model are:

- Density
- Modulus of elasticity in two directions (E)
- Shear modulus in thx-y plane where the material lays (G_{12})

- Longitudinal tensile strength (σ_1)
- Transverse tensile strength (σ_2)
- Shear strength (S_{12})
- Transverse compressive strength (C_2)
- Nonlinear shear stress parameter (α)

While the tensile strength properties were obtained from the tension tests of each material, the material properties for shear and compression were obtained by performing sensitivity analysis on the model.

From experimental testing, it was found that both GN2118 and AS299 have very similar properties in the x and y directions. Hence the constitutive matrix for an orthotropic material in plane stress is simplified to

$$C = \begin{bmatrix} \frac{1}{E_1} & -\frac{v_{21}}{E_2} & 0 \\ -\frac{v_{12}}{E_1} & \frac{1}{E_2} & 0 \\ 0 & 0 & \frac{1}{G_{12}} \end{bmatrix} \tag{3.1}$$

where $E_1 = E_2$ and $v_{12} = v_{21}$.

There are three failure criteria for this model - matrix cracking, compression, and fiber breakage. The values for *E*, *G*, and ν for the elements which meet the failure criteria are set to zero.

A ratio between the shear stress to the shear strength which for this model is defined as

$$\tau = \frac{\frac{\tau_{12}^{\ 2}}{2G_{12}} + \frac{3}{4}\alpha\tau_{12}^{\ 4}}{\frac{S_{12}^{\ 2}}{2G_{12}} + \frac{3}{4}\alpha S_{12}^{\ 4}}$$

The matrix cracking failure criteria is calculated and checked using

$$F_{matrix} = \left(\frac{\sigma_2}{S_2}\right)^2 + \overline{\tau} \tag{3.2}$$

Failure is reached if $F_{matrix} > 1$.

The compression failure criterion is given as

$$F_{comp} = \left(\frac{\sigma_2}{2S_{12}}\right)^2 + \left[\left(\frac{C_2}{2S_{12}}\right)^2 - 1\right]\frac{\sigma_2}{C_2} + \overline{\tau} \tag{3.3}$$

If $F_{comp} > 1$ failure is assumed.

Finally the fiber breakage failure criteria is checked using

$$F_{fiber} = \left(\frac{\sigma_1}{S_1}\right)^2 + \overline{\tau} \tag{3.4}$$

If $F_{fiber} > 1$ failure is assumed.

3.2 Tension tests for fiber resin composites

3.2.1 Objective

A series of tension tests are carried out to determine the ultimate tensile strength and modulus of elasticity for GN2118, AS299, and AS400. This test method is designed to produce tensile property data for material specifications in research and development of body-armor. Several factors that influence the tensile response include: specimen preparation, environment of testing, specimen alignment, gripping pressure, and speed of testing. Properties obtained from this test method, in the direction of testing include the following:

(a) Ultimate tensile strength

(b) Ultimate tensile strain

(c) Modulus of elasticity

3.2.2 Apparatus and Experimental Setup

The tension tests were conducted in a 22 kips servo-hydraulic test frame. The tension tests were conducted in a 22 kips servo-hydraulic test frame. Two styles of flat steel plates 2.5" wide, 2" long, 0.25" thick were used to grip the specimen at both ends. Figure 3-4 shows a typical test setup.

For the GN2118 material, one of the steel plates at each end has a curved groove at the center of the plate throughout its width, which is half the thickness of the plate. The other plate has a V-notch cut in the same position about half the thickness of the plate. A round aluminum rod is cut along the length to the shape of the groove to match the existing grooves in the steel plate. The fabric was held between the V-notch and the aluminum piece so that the notch pinches against the fabric and prevents from slipping with respect to the end plates. The gripping system for GN 2118 is shown below in Figure 3-5.

For AS299 and AS400 flat steel plates 2.5" wide, 2" long, 0.25" thick are used to grip the specimen at both ends. The inside surface of the plates, where the material is placed, has a rough finish to prevent slipping with respect to the end plates. The fabric was held between the plates and the two plates were pressed with hydraulic grips thereby ensuring uniform pressure application to minimize, if not prevent, any fabric slipping. The gripping system for AS299 is shown below in Figure 3-6.

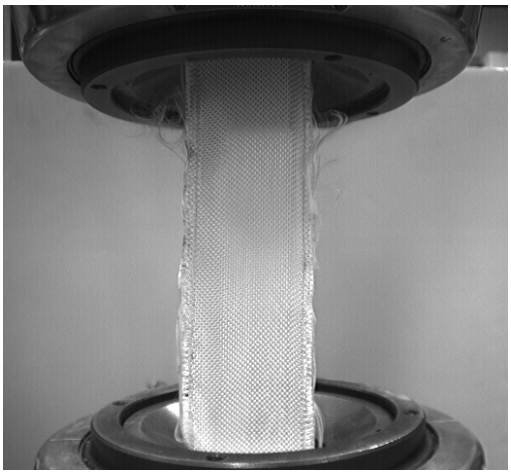

Figure 3-4: Typical Test Setup with Fabric Sample

Figure 3-5: Specimen Gripping System for GN 2118

Figure 3-6: Specimen Gripping System for AS299

3.2.3 Test Procedure

Each sample was cut to approximately 11 in by 1.5 in. The grip length on each side was 2 in while the gage length was approximately 8 in. The testing was conducted per ASTM D 3039 [47]. The rate of displacement of actuator (stroke), as per ASTM standards, was set at 0.1 in/min. The two plates were pressed with hydraulic grips thereby ensuring uniform pressure application to minimize, if not prevent, any fabric slipping. Digital data acquisition was used to collect data at every 0.5 second. The test was continued until complete failure of the specimen was achieved.

3.2.4 Tension Properties Calculations

Before testing each specimen gage length, width, and thickness of the specimen is measured at five different locations. The average values for each dimension are used in calculating the stress and strain values at each point of the recorded data as follows

$$\sigma_i = \frac{F_i}{A_{avg}} \text{ for } i = 1, 2, ..., n \tag{3.1}$$

$$\varepsilon_i = \frac{\delta_i}{L_{gage}} \text{ for } i = 1, 2, ..., n \tag{3.2}$$

where

- F_i is the load at ith data point
- A_{avg} is the average cross-sectional area of specimen
- δ_i is the extensometer displacement at ith data point
- L_{gage} is the average gage length of the specimen

The ultimate strength of the material presented in the results below is the maximum stress from the stress-strain curve in the raw data. The ultimate strain is the corresponding strain at maximum stress.

3.2.5 GN2118 Results

The testing results of GN2118 material are presented below in Table 3-1 and Figure 3-7.

Table 3-1: GN 2118 Tension Test Results

Specimen #	Ultimate Stress (ksi)	Ultimate Strain (in/in)	Modulus of Elasticity (Mpsi)
1	105.3	0.025	4.32
2	101.7	0.025	4.21
3	77.4	0.021	4.09
4	101.6	0.024	4.30
Average	91.1	0.023	4.23

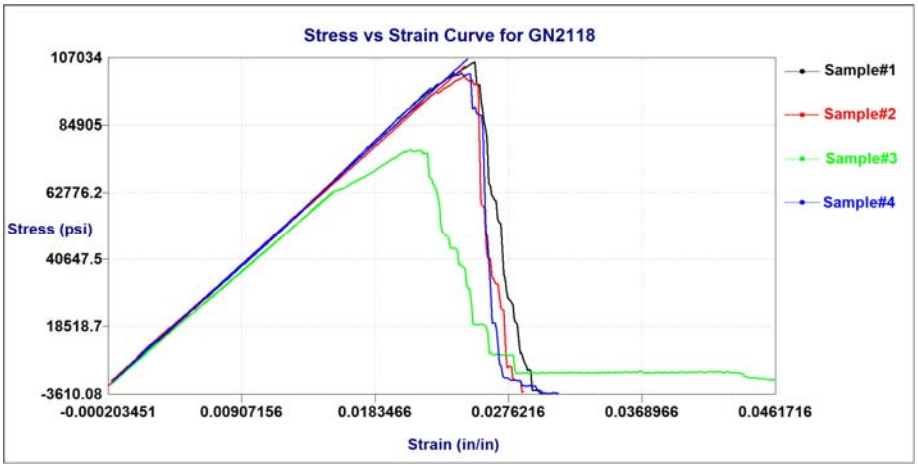

Figure 3-7: Stress/Strain Curves from GN2118 Samples

The above stress strain graphs were analyzed for the pre-peak region only. The pre-peak region of the curve represents the portion of the curve from initial loading to ultimate stress. This region was fitted with a linear polynomial for each sample and the modulus of elasticity reported is the slope of that curve.

3.2.6 AS299 Results

The testing results of AS299 material are presented below in Table 3-2 and Figure 3-8. The tests were performed with a gripping pressure of 1.4 MPa (200 psi).

Table 3-2: AS299 Tension Test Results

Sample #	Ultimate Stress (ksi)	Ultimate Strain (in/in)	Modulus of Elasticity (Mpsi)
1	64.7	0.030	2.18
2	67.8	0.031	2.27
3	61.8	0.031	2.03
4	60.8	0.030	2.02
Average	63.8	0.030	2.12

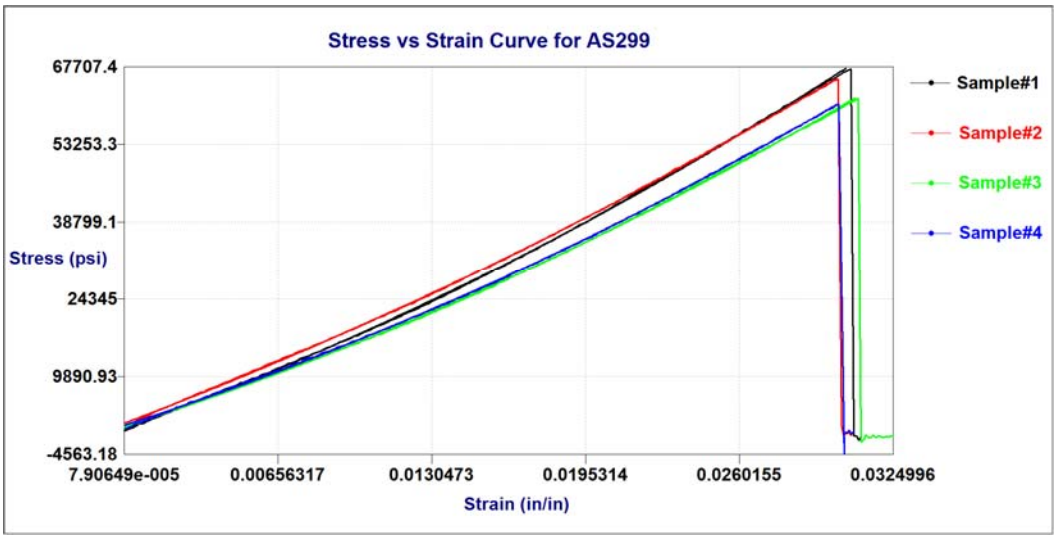

Figure 3-8: Stress/Strain Curves from Raw and Best Fit Data of AS299

Similar to GN2118 material results, the pre-peak region of the stress strain curve is fitted with a linear curve and the modulus of elasticity is found from the slope of best fit line.

3.3 Foam Compression Test

3.3.1 Objective

A series of loading-unloading compression tests were carried out to determine the behavior of the material at different levels of compression for vinyl nitrile foam. This test is used to classify the foam as open-celled and the results of this test are used to as input data in a FEA material foam model. Several factors that influence the compression response include: compression percentage, specimen preparation, environment of testing, and specimen alignment.

3.3.2 Apparatus and Experimental Setup

The compression test was performed using Instron 4411 machine. This is a 1000lb load capacity electromechanical materials testing machine with a stationary base plate and a moving crosshead with a mounted load cell. The sample was set on a fixed base and covered by an aluminum thin plate with dimensions. The load cell pushed on the aluminum plate, which in return compressed the foam samples evenly. A picture of a sample set-up is shown below in Figure 3-9.

Figure 3-9: Compression test set-up

3.3.3 Test Procedure

ASTM 1056-07 [48] standards were followed for testing this foam. The first test was done for 25% deflection of the specimen. A rate of 15 mm/min was used to compress the specimen. Based on the average thickness of the specimen, which was found to be 0.327in over 9 samples tested, the machine unloaded the sample when a 25% compression deflection was reached, i.e. the sample was deflected 0.0817in. The process was repeated until the loading and unloading loads did not vary more than 5%. Sample deflections and load were recorded using the Instron machine. Once the compression reached 25% the process was repeated (cyclic loading) until the loads did not vary more than 5%.

3.3.4 Compressive Properties Calculations

The compressive stress and strain were measured using the following formulas

$$\sigma_C = \frac{Load}{Comp.Area}$$
$$\varepsilon_C = \frac{Stroke}{SampleThickness} \tag{3.3}$$

3.3.5 Results

This loading unloading test was done on nine samples. Three samples at a time were tested for compression levels on the thickness of the sample to be 25%, 50%, and 75%, respectively. The results of these tests are shown below in Figure 3-10, Figure 3-11, Figure 3-13, and Figure 3-13 below. Also, to show that the initial loading is independent of the compression level, Figure 3-13 shows three samples compressed 25%, 50%, and 75% respectively.

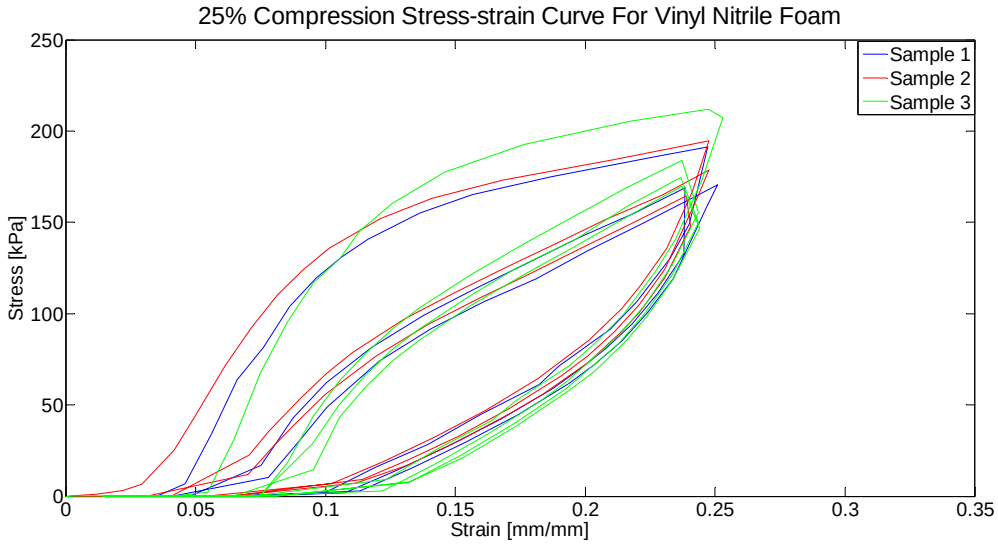

Figure 3-10: 25% compression on overall thickness of foam samples

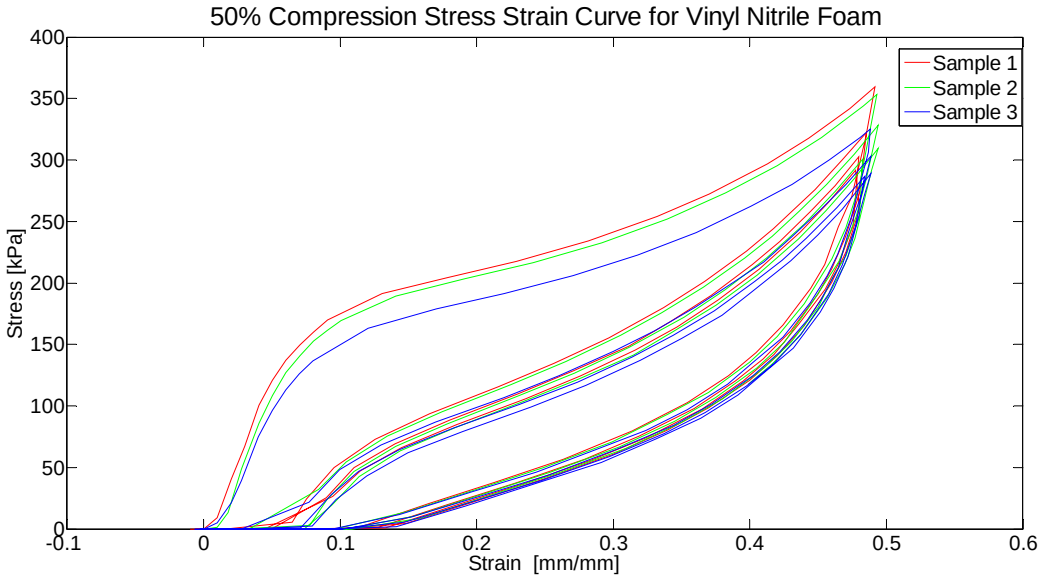

Figure 3-11: 50% compression on the overall thickness of foam samples

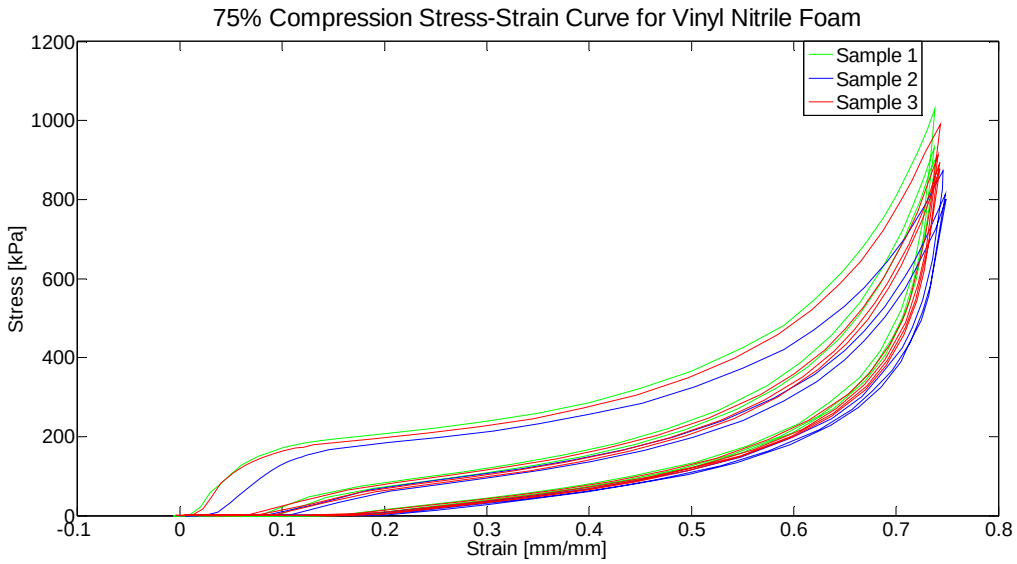

Figure 3-12: 75% compression on the overall thickness of foam samples

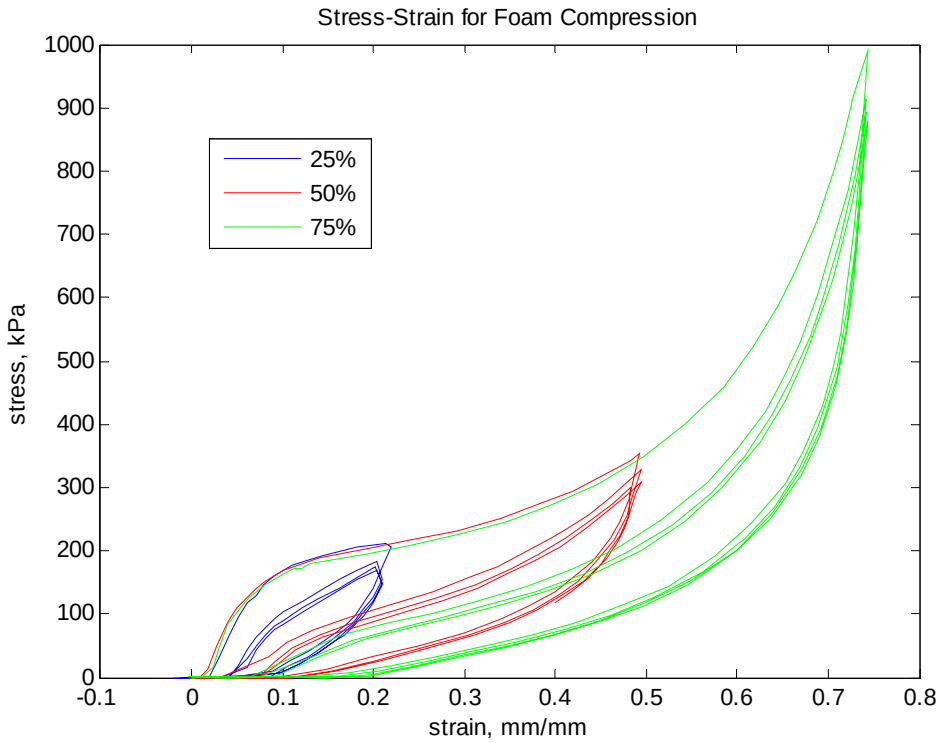

Figure 3-13: Stress-strain curve for 25%, 50%, and 75% sample thickness compression

3.4 Drop-sphere Test as Means of Validation of Material Models

3.4.1 Overview and significance

The drop-sphere test involves dropping a steel sphere to a known material from a known height and measuring the rebound height of the sphere. A series of these tests were carried out to validate material models in LS-DYNA used for steel, foam, GN2118, and AS299 materials. The size of the sphere, the drop-height, and the number of layers of the material were varied to test the response of the material. For the test, a sphere was dropped on the appropriate material underlined with a steel plate and the maximum rebound height was measured. Several factors that influence the drop test include the height of drop, test environment, and the number of pixels in each image.

3.4.2 Apparatus

A Phantom high speed camera was used to record the motion of the ball at 2000 frames per second. The camera was connected to a data collecting computer to record testing results. For each test, a string was tied around the columns of the drop machine at 250 mm height from the top surface of the material being tested and used as a reference line needed to specify a known distance when processing experimental data. A laser level as shown in Figure 3-14(a) below was used to align the string and the reference lines of the camera in the phantom software. Two tests for each of the three drop-heights were performed. Figure 3-14 below shows the test set-up.

Figure 3-14: (a) Camera and laser level set-up; (b) testing machine and reference string

3.4.3 Test Procedure

The material tested for maximum rebound height is placed on a flat steel base surface. The height between the top surface of the material and the location from which the ball is dropped is measured and set to the required height. Once the steel sphere is dropped, the camera is triggered and frames are recorded at the specified frame rate.

3.4.4 Processing Experimental Data

The analysis of the experimental data was done using the measuring option in the Phantom camera software. Before numerical data was collected, units, origin, and a known distance in the frame, in this case the string tied around

the drop frame columns, were specified. Data was recorded by clicking the center of the sphere every 10ms.

3.4.5 Results for steel

A sphere size of 28 mm was used for this test only. The spheres were dropped from three different heights, as shown in Table 3-3.

Table 3-3: Steel test results for drop-sphere test

Test	Drop-Height (mm)	Avg. Experimental Displacement (mm)
1	381	94.0
2	508	118.9
3	635	156.7

3.4.6 Results for foam

Three different cases of foam arrangements were tested. The results for the number of layers of foam tested with a 25 mm sphere as well as the maximum bounce height are displayed in Table 3-4. Comparing foam drop-test results to the steel results it can be observed that, as expected, foam absorbs the impact energy more than steel and hence the maximum bounce height is less for foam than steel.

Table 3-4: Foam test results for drop-sphere test

Number of Foam Layers	Drop-Height (mm)	Maximum Bounce Height (mm)
1	508	32.4
	635	38.9
2	508	41.5
	635	51.6
4	492	42.8
	635	56.2

3.4.7 Results for GN2118 and AS299

A drop height of 635 mm and sphere size of 25mm was used for measuring the rebound height of GN2118 and AS299. Graphical and tabulated results are provided below in Figure 3-15, Figure 3-16, and Table 3-5, respectively.

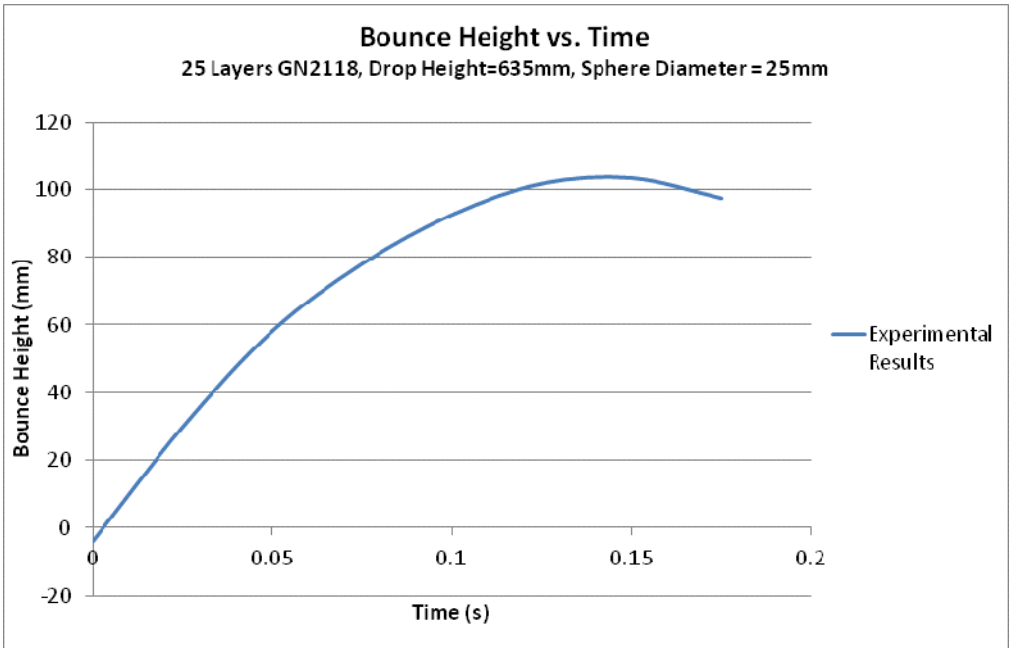

Figure 3-15: GN2118 drop-test results

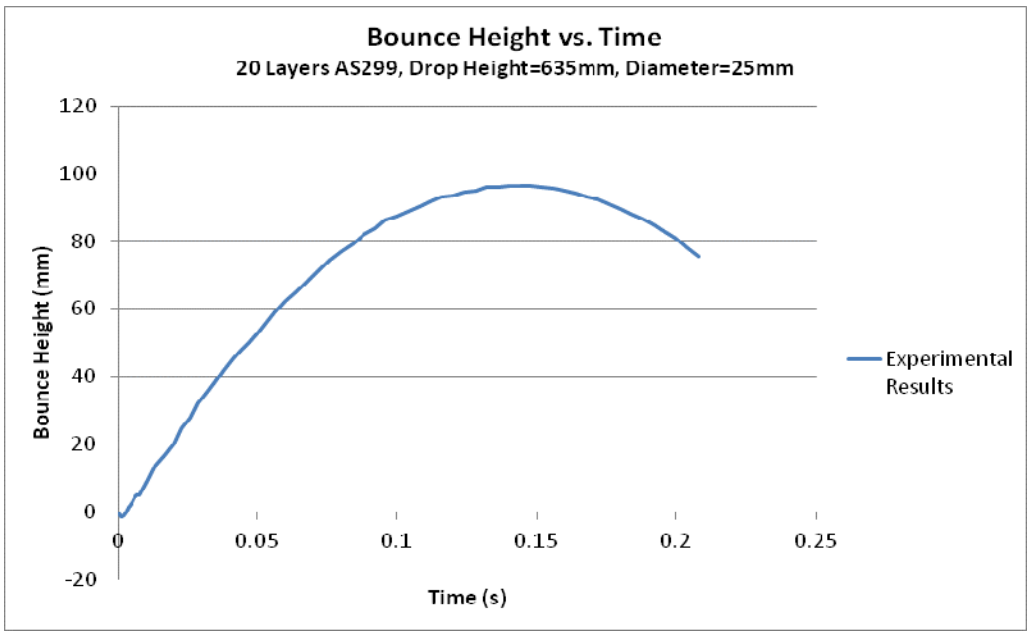

Figure 3-16: AS299 drop-test results

Table 3-5: GN2118 and AS299 test results for drop-sphere test

Material Type	Drop Height (mm)	Maximum Bounce Height (mm)
GN2118	635	104
AS299	635	96

3.5 Knife and Spike Test

3.5.1 Objective

The objective of this test is to measure the depth of penetration in layers of different configurations of AS299, GN2118, and AS400 material in research of body armor. The test followed guidelines specified in the NIJ standards to the best ability that the laboratory and available equipment allowed. Witness paper was inserted between the sample and backing material to measure the length of the cut. The penetration depth was than measured by consulting Appendix C table in the NIJ standard.

3.5.2 Apparatus and Test Setup

ASU has a drop test set-up based on a free-fall drop of an instrumented hammer. A picture of the system is shown below in Figure 3-17. The different components of the machine are:

- Free weight – built-in part with frictionless bearings of the machine where the knife or spike are attached on
- Base plate – a steel base plate where the backing and composite material are placed upon
- Knife and spike frame – frame in which knife and spike were attached via an Allen bolt
- Witness paper - placed between the armor and the top layer of the composite backing material to determine if penetration of knife took place of not. A relationship between the depth of penetration of the knife and the length of the cut on the witness paper is given in Appendix D of the NIJ standards.

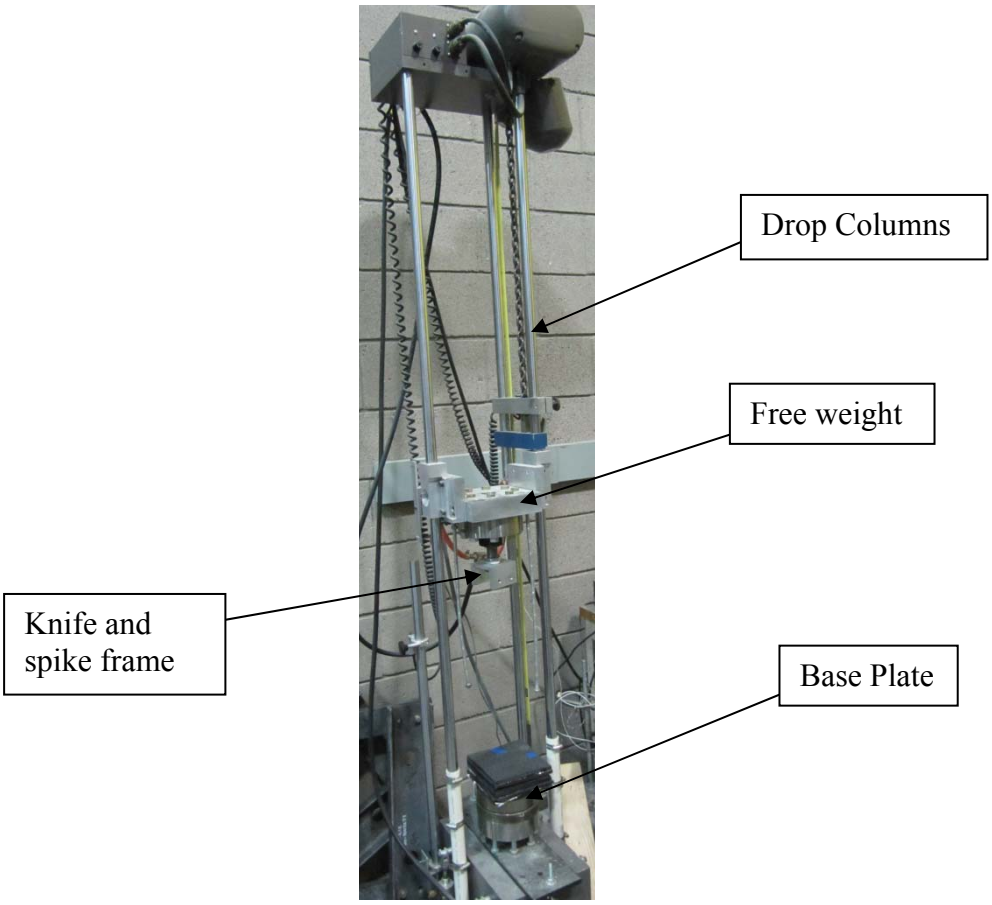

Figure 3-17: Drop Test Machine and Its Components

The free weight that dropped on the target material was measured to be 26 lb (116 N). Based on the weight of the assembly the corresponding change in height satisfying NIJ standards for protection level one and energy levels one and two are shown in

Table 3-6 below. These values were obtained by assuming that the kinetic energy is equal to potential energy. So, the change in height was calculated as

$$E = mg\Delta H$$
$$\Delta H = \frac{E}{mg} \tag{3.4}$$

Table 3-6: Energy level and corresponding heights for the drop-test set-up at ASU

Energy Level	Corresponding ΔH (mm)
E_1=24J	207
E_2=36J	311

The drop height can be controlled by means of an electronic hoist and release mechanism as shown in Figure 3-18. The backing material used is vinyl-nitrile foam. The backing material is attached to the base plate where the specimens are set-up by attaching adhesive to the plate and the foam as shown in Figure 3-19.

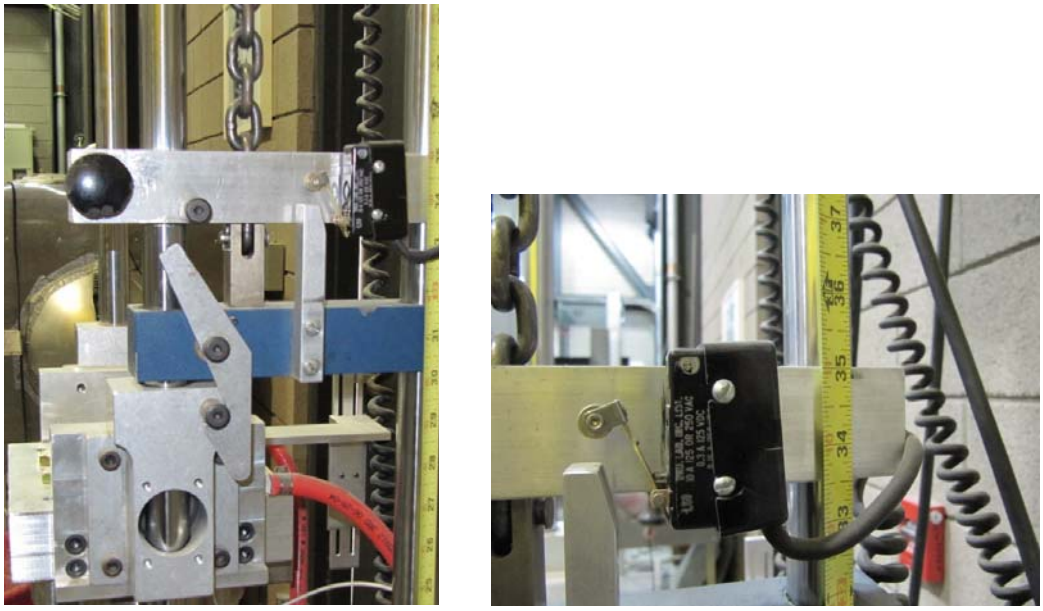

(a) (b)

Figure 3-18: (a) Height control mechanism, (b) Release mechanism

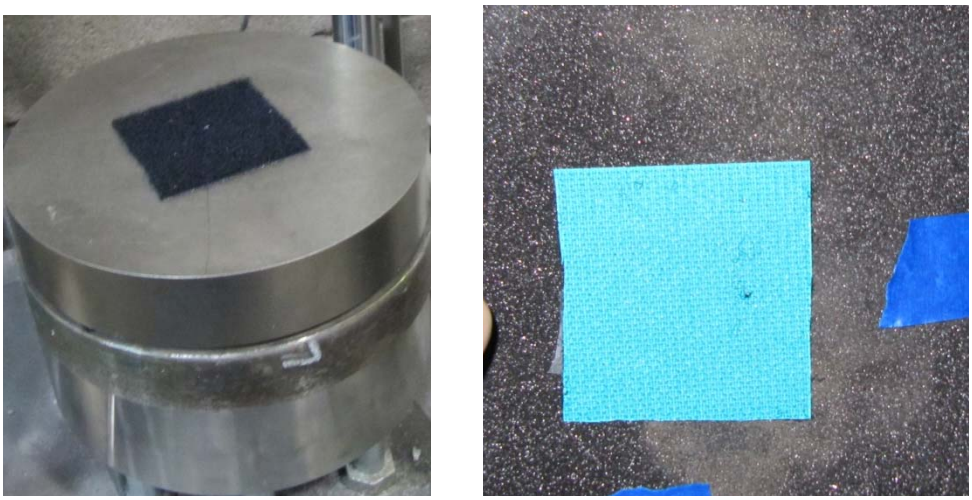

(a) (b)

Figure 3-19: (a) Adhesive attached to the base plate, (b) Adhesive attached to the backing material

The knife or spike is attached to the drop test set up by means of an aluminum block and a bolt inside the block which keeps the knife and spike in place. The block dimensions are of 75 mm x 50 mm x 35 mm. The block and the instrument are then mounted to the testing frame through Allen bolts. A picture of this set up is shown in Figure 3-20 below.

Figure 3-20: Ready to test spike set-up

The sample size of the foam and the material tested were 8 in by 8 in. These are the maximum allowable dimensions that the current drop machine allows. To run the test, the trigger releases the hoist by pressing the release mechanism button in the machine.

3.5.3 Results and Discussion

Two samples were tested with the following material configurations.

Table 3-7: Knife and Spike Test, Sample 1

Material	Areal Density lb/ft^2	Sample Size ft^2	Number of Layers	Weight Total lb
AS299	0.03	0.44	20	0.30
GN2118	0.04	0.44	25	0.25
Total Areal Density (lb/ft^2):				1.24
Actual Sample Weight (lb)				0.54
Actual Areal Density (lb/ft^2):				1.22

Table 3-8: Knife and Spike Test, Sample 2

Material	Areal Density lb/ft^2	Sample Size ft^2	Number of Layers	Weight Total lb
GN2118	0.04	0.44	25	0.25
AS299	0.03	0.44	12	0.18
AS400	0.06	0.44	1	0.03
AS299	0.03	0.44	12	0.18
Total Areal Density (lb/ft^2):				1.43
Actual Sample Weight (lb)				0.63
Actual Areal Density (lb/ft^2):				1.43

Pictures of sample 2 before and after it is tested are shown in Figure 3-21 and Figure 3-22 below.

Figure 3-21: Sample set-up before testing with energy level 1

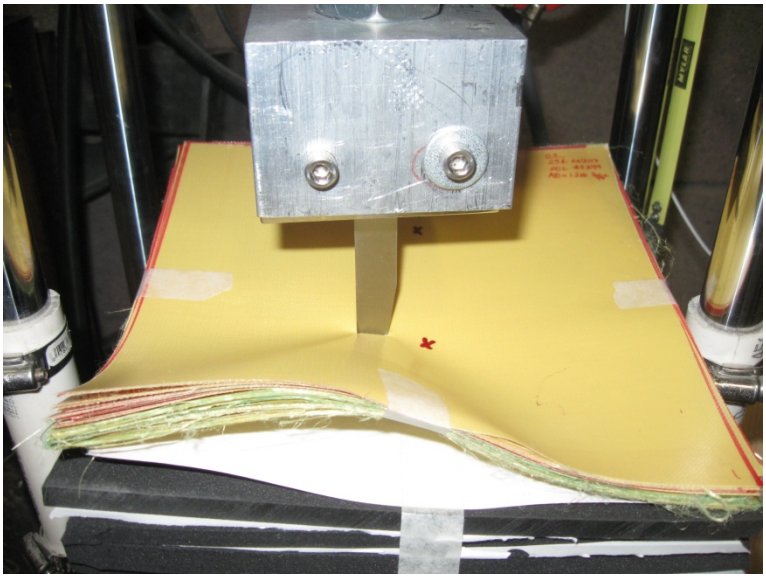

Figure 3-22: Sample after knife test

Both samples were tested with two different energy levels (24 J and 36 J). The numbers of knife and spike tests for this sample were four. The results of the Arizona State University tests are summarized below in Table 3-9. Pictures

depicting the material damage at every tenth layer of each sample are shown in Appendix B.

Table 3-9: Knife and Spike Test Results

Sample	Energy Level (J)	Drop Height (mm)	Length of cut on witness paper (mm)	Depth of penetration (mm)
1	24	207.4	5.66	13.1
	36	311.1	9.37	22.02
2	24	207.4	4.9	11.3
	36	311.1	7.12	16.6

3.6 Discussion of the experimental test results

As can be observed from the uniaxial tension test, GN2118 has a higher tensile strength and modulus of elasticity than AS299. However in response to the knife test AS299 absorbs the impact energy better than GN2118. This is because GN2118 has a poor adhesion to the gold shield attached to aramid fiber in this material allowing the knife and spike to easily penetrate and not provide good stab protection. This material is mainly used for ballistic protection where the delamination of the material is an advantage [49].

On the other hand, AS299 shows better ability to absorb impact energy. This is best seen in the drop-sphere test, where the rebound height of the steel sphere is lower for AS299 then for GN2118. AS299 has epoxy on top and bottom of the aramid fibers, leaving little room for knife to penetrate through, and hence making it a better choice for stab protection.

4. FINITE ELEMENT ANALYSIS OF THE KNIFE AND SPIKE AND DROP-SPHERE TESTS

A description of the knife and drop-sphere model and the necessary keywords to build them in LS-DYNA FEA software are provided in this chapter. Numerical Results of the finite element analysis including the calibration of the model and the drop-sphere test are also presented.

4.1 Explicit Finite Element Analysis

Simulating dynamic and quasi-static deformations which are linear or non-linear and might have complex impact problems requires the use of either implicit or explicit solution, both which are numerical integration techniques in finite element analysis. Examples of these types of analysis include crashworthiness analysis, drop testing, metal forming, etc.

Implicit method is used in quasi-static problems, in which case the solution is unconditionally stable for large time-steps. This technique solves differential equation implicitly. In other words displacement at any time-step is solved by obtaining a system of equations and through an iterative process the solution is achieved at that time step. This is a well suited technique for static and quasi-static simulations. The advantage of this technique is that usually solution is obtained in less number of time-steps than the explicit analysis techniques.

Explicit technique is a well suited method of dynamic and crash simulations where time of the event is brief as well as for highly nonlinear problems involving contact definitions. It assumes linear change in displacement over each time step and it is stable only if time step is smaller than the critical

time step. This technique is suitable for modeling brief, transient dynamic event such as impact and blast problems [50]. Since this technique doesn't require inverting stiffness matrix, it requires less computer memory storage. However, the solution is only conditionally stable. To ensure stability, many times, the time step needs to be very small and hence the number of time steps required to obtain the solution might be very large, which can be costly.

The governing differential equations solved for any non-linear finite element problems, which include explicit and implicit solving techniques, are:

(1) Conservation of mass

(2) Conservation of energy

(3) Conservation of momentum

(4) A measure of deformation relates strain to displacement

(5) A constitutive equation which relates measure of deformation to stress

4.2 Knife and Spike Model Description

The knife and spike LS-DYNA model consists of nine parts, modeling the experimental drop test. These parts consist of:

(1) Drop weight attached to the knife or spike

(2) Engineered knife (Appendix C)

(3) Engineered spike (Appendix C)

(4) Two layers of AS299 with a thickness equivalent to twenty layers of AS299

(5) Two layers of GN2118 with a thickness equivalent to twenty five layers of GN2118

(6) Two Layers of foam with a thickness equivalent to four layers of foam

(7) Steel plate fixed at the bottom.

The engineered knife and spike dimensions were based on the NIJ standards Appendix C. The material composites and drop-weight block dimensions matched the actual samples used in experimental testing at ASU structures lab. Each part was modeled in SolidWorks [51] and meshed in HyperMesh [52]. While the rigid mass, foam, and steel plate are modeled using solid elements, the engineered knife and the dry fabrics are modeled using shell elements. The target material consisting of the fiber resin composites, foam, and steel plate have a finer mesh toward the center where the knife was predicted and observed to hit. Figure 4-1 below shows the different parts in the knife and spike model as well as the overall models. Table 4-1 shows the number of node, the element type, and the number of elements for each part.

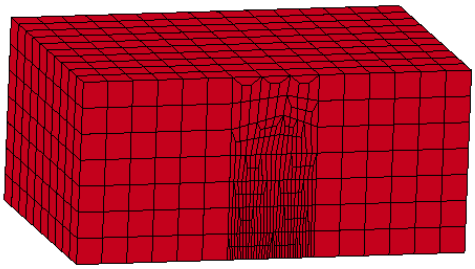

(a) Drop weight block part and its mesh

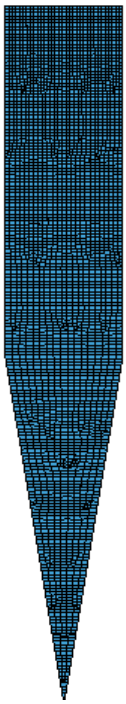

(b) Knife part and its mesh

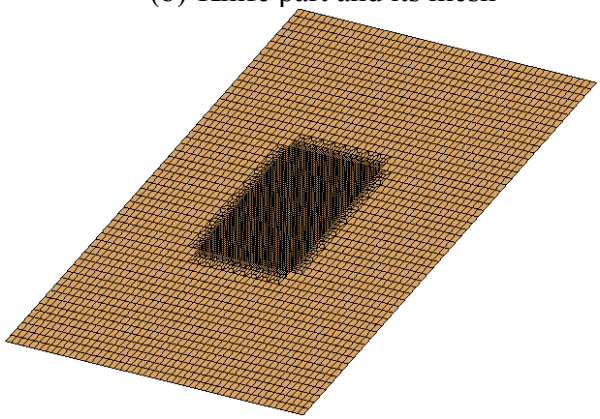

(c) Composite part and its mesh

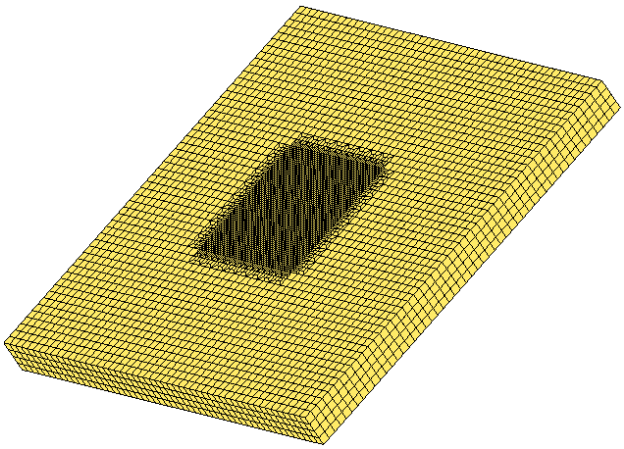

(d) Foam part and its mesh

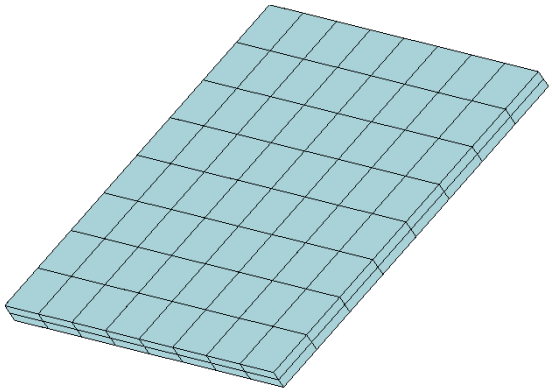

(e) Steel plate part and it's mesh

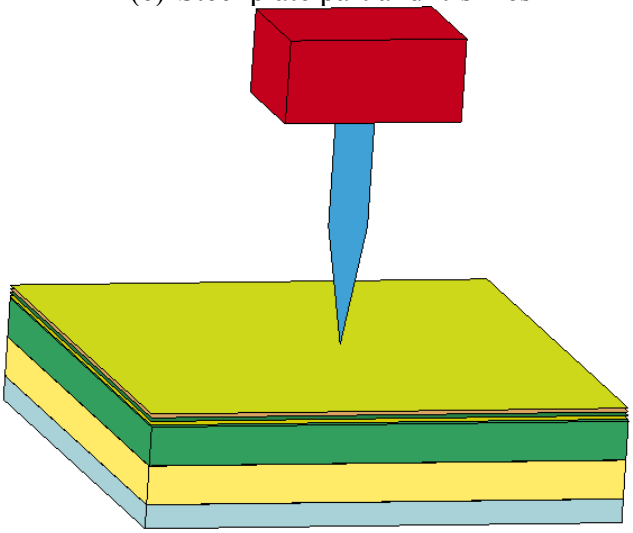

(f) Overall knife and target material model

Figure 4-1: Knife model parts and their mesh

Table 4-1: Number of nodes, element type, and number of elements for each part in the knife model

Part	Number of Nodes	Elementy Type	Number of Elements
1st Layer of AS299	7097	Belytschko-Tsay shell elements	6992
2nd Layer of AS299	7097	Belytschko-Tsay shell elements	6992
1st Layer of GN2118	7097	Belytschko-Tsay shell elements	6992
2nd Layer of GN2118	7097	Belytschko-Tsay shell elements	6992
1st Layer of Foam	35485	Constant stress solid element	27968
2nd Layer of Foam	35485	Constant stress solid element	27968
Steel Plate	243	Constant stress solid element	128
Knife	3946	Belytschko-Tsay shell elements	3755
Block	3817	Constant stress solid element	3090

4.3 Element types and definition

Shell elements are used to define the armor fabrics and the knife. Three and four noded Belytschko-Tsay elements were used with two through shell thickness integration points [53].

The steel block connected to the knife, spike, and the backing material (foam and steel plate) are modeled using 8-node hexahedron elements. Reduced integration is used and the stress is calculated at the center of the element.

4.4 Contact definition

The contact definition specified between each layer of material and between the knife and the target materials in LS-DYNA is *AUTOMATIC_SURFACE_ TO_ SURFACE contact. The automatic option detects penetration coming from slave or master part, automatically [54]. For both the drop-sphere test and the knife model, the slave part is specified to be the target material and the master part is the sphere or knife, respectively. When very soft materials, such as foam and the dry fabrics, are in contact with a stiff material such as steel, they may lower the contact stiffness value and cause excessive penetration. To solve this, a soft constraint penalty formulation is used in both drop-sphere and knife and target material models. No dynamic or static friction coefficients are defined for either of the models.

4.5 Hourglass energy definition

When solid shells with one integration point solid elements and shells are used in a model, hourglass modes occur. These are zero-energy modes of

deformation that produce zero strain and stress. The value of these modes for all parts needs to be relatively small.

For the knife part, an hourglass type 8 was selected. This control type of hourglass applies to shell elements type 16 only. It activates a warping stiffness so that warping of elements during contact does not degrade solution.

4.6 Material validation

The validation of each material model was done using a drop-sphere test. For each drop test, the sphere and the target material were modeled to be in a very close proximity to each other. The results presented below correspond to a sphere size of 25 mm meshed using 3D elements. Figure 4-2 below shows the steel sphere used for the drop-test models.

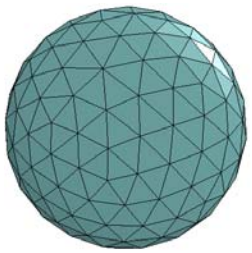

Figure 4-2: Steel sphere mesh

The initial velocity of the sphere was specified based on the experimental test drop height. Assuming that kinetic energy immediately before the sphere is in contact with the target material is equal to the potential energy, the initial velocity of the sphere was calculated as follows

$$v = \sqrt{2g\Delta h} \tag{4.1}$$

where v is velocity, g is the gravitational acceleration, and Δh is the drop height (distance between the top surface of the test material and location of the drop on the steel plate).

Similar to the overall knife and spike model an automatic surface to surface contact, initial velocity, and solid section were specified for the drop-sphere model. In order to replicate gravitational acceleration, which causes the sphere to drop after rebound, a global acceleration was defined via keyword *LOAD_BODY_Z. To damp low-frequency structural modes present in impact models such as the drop-sphere test, a global damping coefficient was also incorporated into the model.

Since the damping coefficient was observed to vary depending on the type of material the sphere was dropped on and since the lowest frequency cannot be estimated this test also served as an effective test to measure the damping coefficient as a material property. The damping coefficient value was adjusted via sensitivity analysis so that the finite element analysis results match the experimental results.

4.6.1 Sphere on steel plate model and results

Steel plate with dimensions of 203 mm by 203 mm was modeled using solid elements and steel material properties. Figure 4-3 below show the overall model at initial time-step as well as at the last time-step before the sphere starts receding from the maximum bounce height. The initial velocity for this model corresponds to a 635 mm drop height.

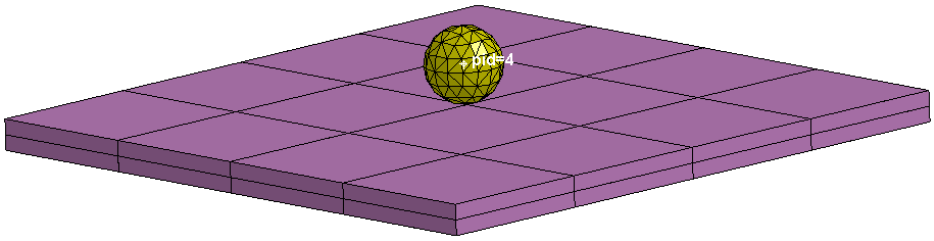

t = 0ms

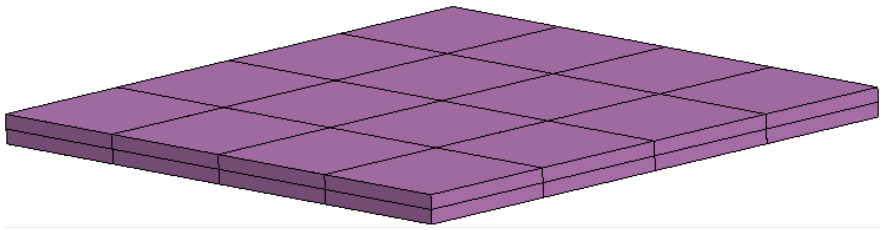

t = 120 ms

Figure 4-3: Sphere drop-test on steel plate at (a) t = 0ms and (b) t=120ms

The optimum damping coefficient for this run was found to be 0.0159. This value was found by doing a regression analysis using different damping coefficients and computing the error between the experimental and FEA bounce heights. Using the least square method, the error is defined as

$$E = \left(\frac{D_{\max}^{FE} - D_{\max}^{Exp}}{D_{\max}^{Exp}} \right)^2 \tag{4.2}$$

where $D_{\max}^{FE}$ is the maximum rebound height from FEA and $D_{\max}^{Exp}$ is the maximum rebound height from experimental testing. Table 4-2 below shows the runs with different damping coefficients and the response from rigid body displacement.

Table 4-2: Sensitivity analysis for a 635 mm drop of steel sphere onto steel plate

Run	DC	Experimental Bounce Height (mm)	FEA Bounce Height (mm)	Error
1	0.01375	146	161	0.011
2	0.015	146	152	0.0017
3	0.016	146	145	0.000047
4	0.0165	146	142	0.00075
5	0.0175	146	135	0.0057

Fitting a second order polynomial to the above data it is found that the damping coefficient which gives the optimum error is 0.0159. Figure 4-4 below shows the experimental and FEA results of the bounce height of the sphere impacting a steel plate. The results show a discrepancy between experimental and FEA results when it comes to rate of change of displacement with respect of time. This can be due to air friction and other environmental factors present during experimental testing which were not included in the FEA model.

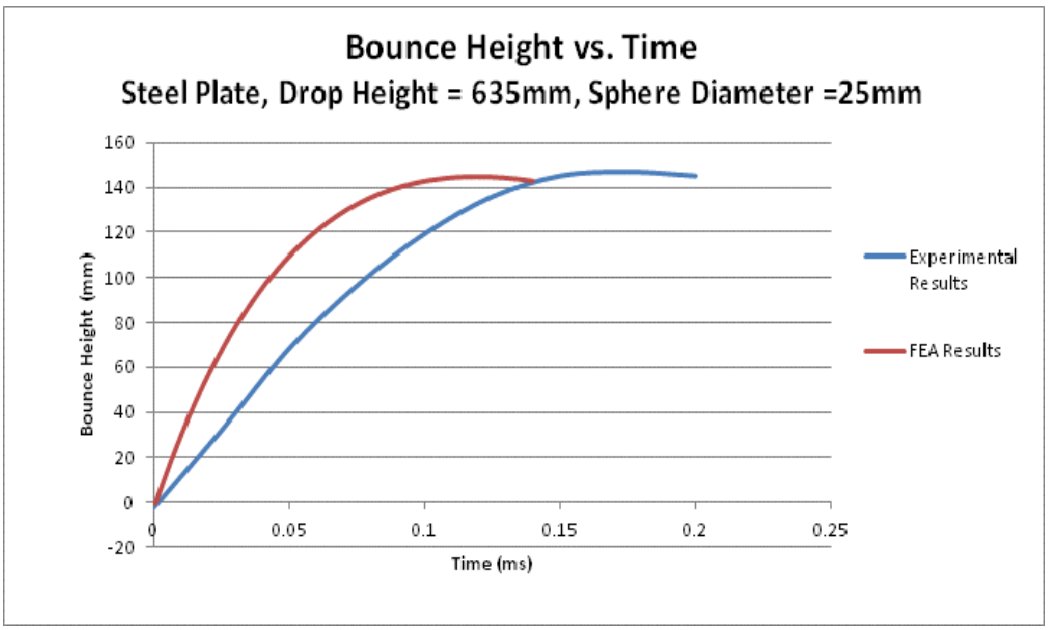

Figure 4-4: Bounce height vs. time for steel plate (635 mm drop height, 25 mm steel sphere)

4.6.2 Sphere on foam model and results

In validating the foam model, two different drop heights were used. The foam is modeled using solid elements. Three foam configurations were used to validate this model. The first model included one layer of foam only. The second model involved two layers of foam. The third model is a two layer model with each thickness being twice the thickness of the foam to represent four layers of foam in total. This was done to cut-down the run-time of analysis.

Figure 4-5 shows the drop sphere model at initial time-step, at the compression stage of the foam, and maximum rebound height.

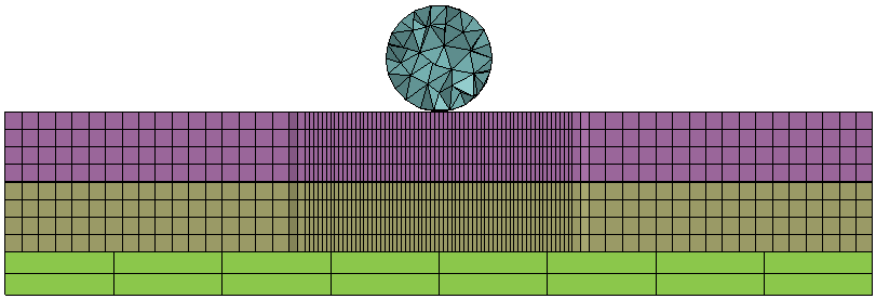

(a) t = 0 ms

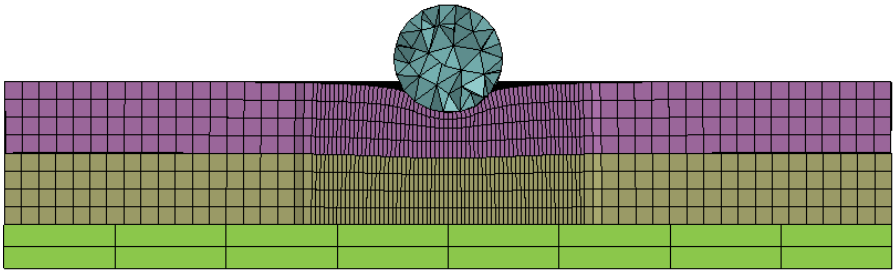

(b) t = 3ms

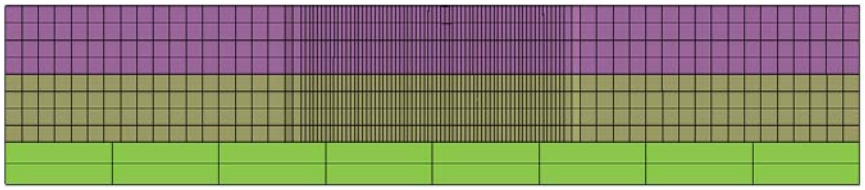

(c) t=80 ms

Figure 4-5: Sphere drop-test on four layers of foam at (a) t = 0 ms and (b) t = 3 ms, and (c) t = 80 ms

Table 4-3: Experimental and FEA test results for drop-sphere test on foam

# of Foam Layers	Drop-Height (mm)	Damping Coefficient	Experimental Maximum Bounce Height (mm)	FEA Maximum Bounce Height (mm)	Percent Difference With respect to Experimental Results
1	508	0.027	32.35	31.87	1.48%
	635	0.027	38.93	35.76	8.14%
2	508	0.02	41.48	44.98	8.44%
	635	0.02	51.59	51.47	0.23%
4	492	0.03	42.79	44.56	4.14%
	635	0.03	56.21	52.57	6.48%

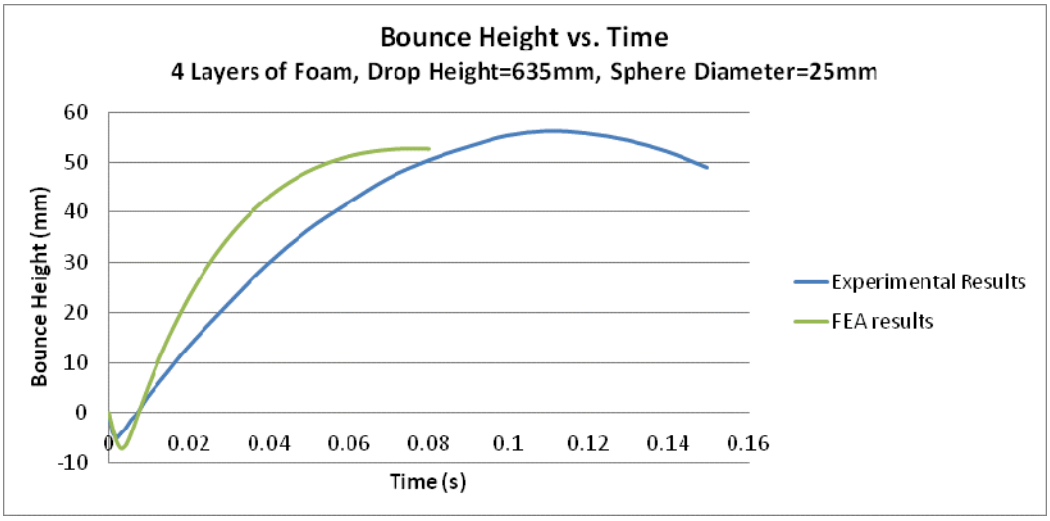

Figure 4-6: Experimental vs. FEA results of drop-sphere test on foam

4.6.3 Sphere on GN2118 and AS299 model and results

When more layers and contact definitions are added to an FEA model, the run-time increases drastically. In trying to match FEA and experimental results for the drop-sphere test involving GN2118 or AS299, foam, and steel plate only one drop height was used to validate the GN2118 and AS299 model due to a large run-time. Both these composites are modeled using shell elements. Similar to the argument for foam, to decrease run-time 25 physical layers of GN2118 are

modeled as 2 layers in LS-DYNA. The first layer has a thickness equivalent to 15 physical layers and the second part of GN2118 has a thickness of 10 physical layers. The 20 physical layers of AS299 are modeled as two shell parts in LS-DYNA, each with a thickness of 10 physical layers.

Figure 4-7 and Figure 4-9 shows the drop sphere model at initial time-step, at the compression stage of the material and foam, and at maximum rebound height for GN2118 and AS299. Figure 4-8 and Figure 4-10 show plots of experimental versus FEA results for a 635 mm drop height. The damping coefficients found to optimize the error between experimental and FEA results for GN2118 and AS299 are 0.014 and 0.016, respectively.

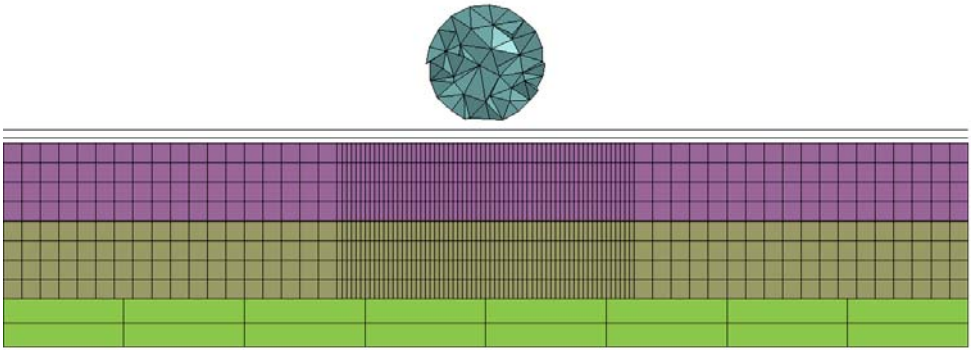

(a) t = 0 ms

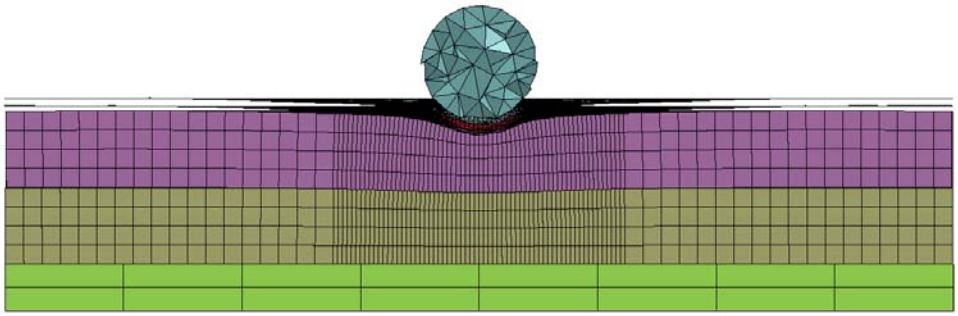

(b) t = 3 ms

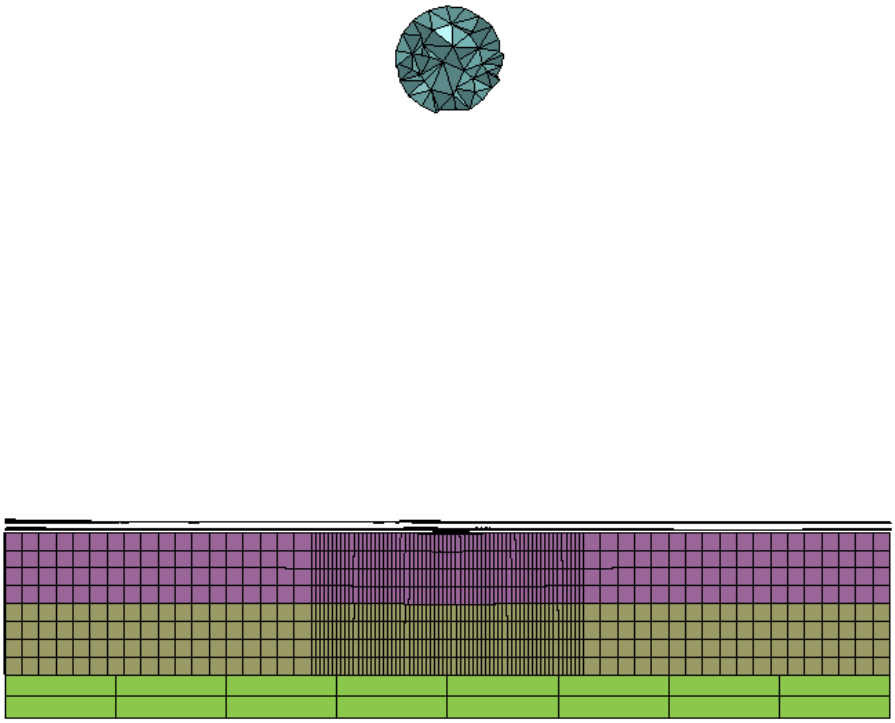

(c) t= 120 ms

Figure 4-7: GN2118 Sphere drop-test on GN2118 at (a) t = 0 ms and (b) t = 3 ms, and (c) t = 120 ms

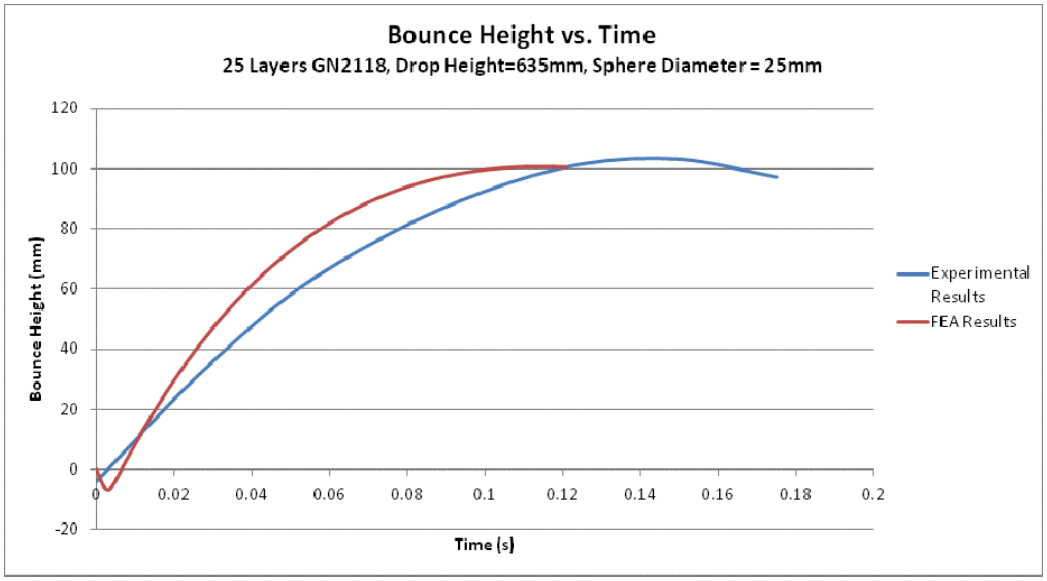

Figure 4-8: Experimental vs. FEA results of drop-sphere test on GN2118

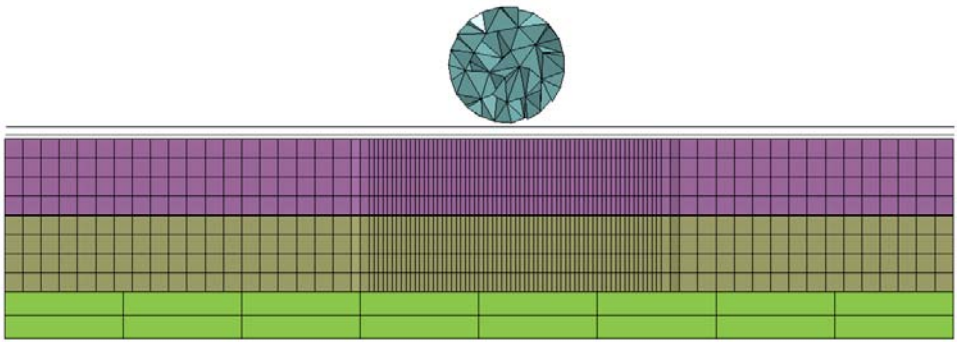

(a) t = 0ms

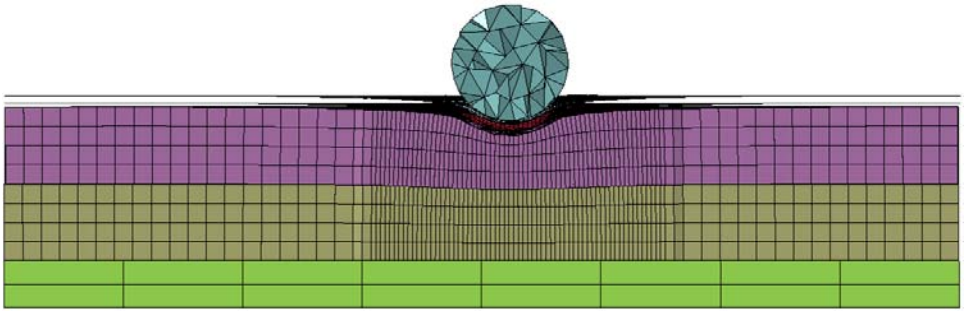

(b) t = 3 ms

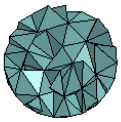

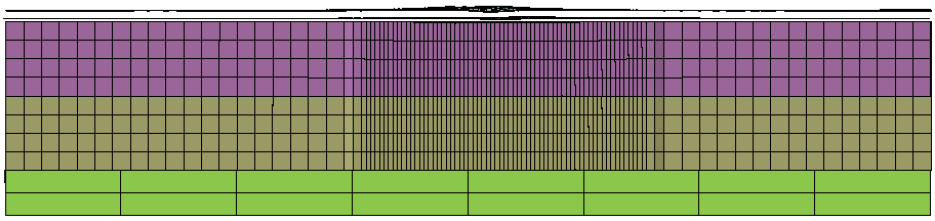

(c) t = 103 ms

Figure 4-9: AS299 Sphere drop-test on GN2118 at (a) t = 0 ms, (b) t = 3 ms, and (c) t = 103 ms

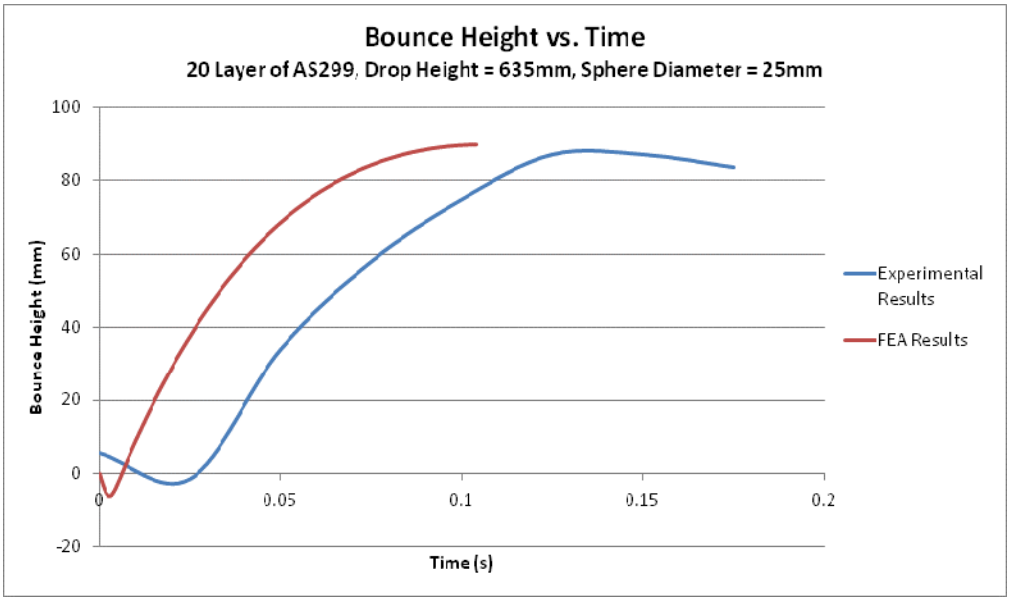

Figure 4-10: Experimental vs. FEA results of drop-sphere test on AS299

4.7 Knife and spike resuls for Approach One Model

In order to match experimental to FEA results in the knife and spike model, the shear modulus, transverse compression strength, and shear strength had to be adjusted by calibrating the model. Multiple runs were made with different values of these material properties. The depth of penetration was the only output component of the model that was analyzed and tried to be matched with experimental data. Due to a complex contact between the knife and composite materials, two different methods were used to obtain a model in which the knife would penetrate through the layers of fabric. In the first model an automatic contact between the knife and the target material was defined. In the second method, nodes where the knife hit the target material were tied and an allowable failure strain was specified. If the allowable strain value was exceeded, the knife would penetrate through the target material.

4.7.1 Knife and spike model with automatic contact definition (Approach One Model)

As mentioned above this method uses the automatic surface-to-surface contact (see section 4.4 Contact definitionfor contact type definition) for all the contact between the differfent parts of the model. By varying shear strength, transverse compressive strength, and shear modulus, meaningful results were attempted to be obtained for this model. Figure 4-11 shows the knife penetration on the composite model after a few time stepa in the FEA analysis. The experimental results of this test are provided in Appendix B.

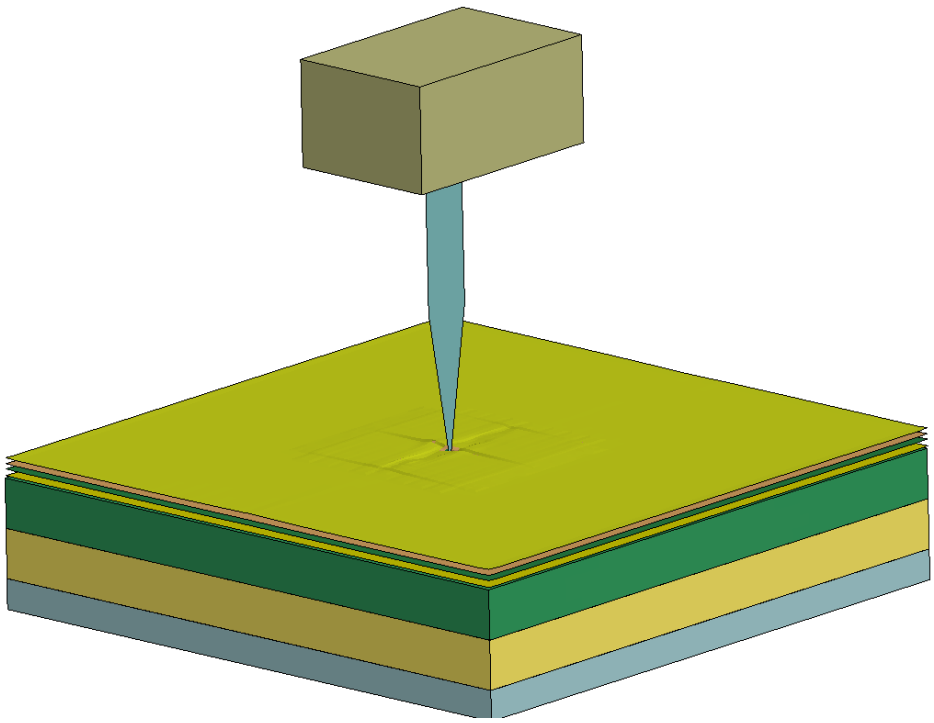

(a) Overall model

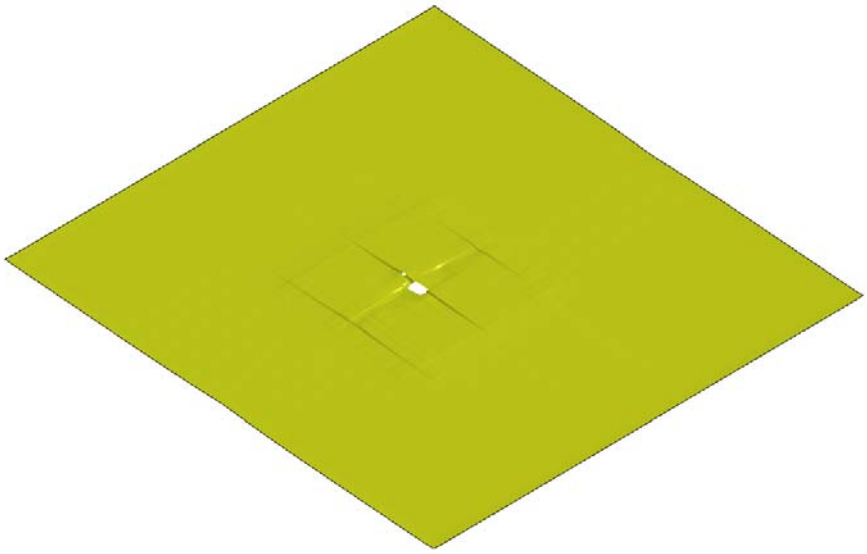

(b) AS299 layer damage

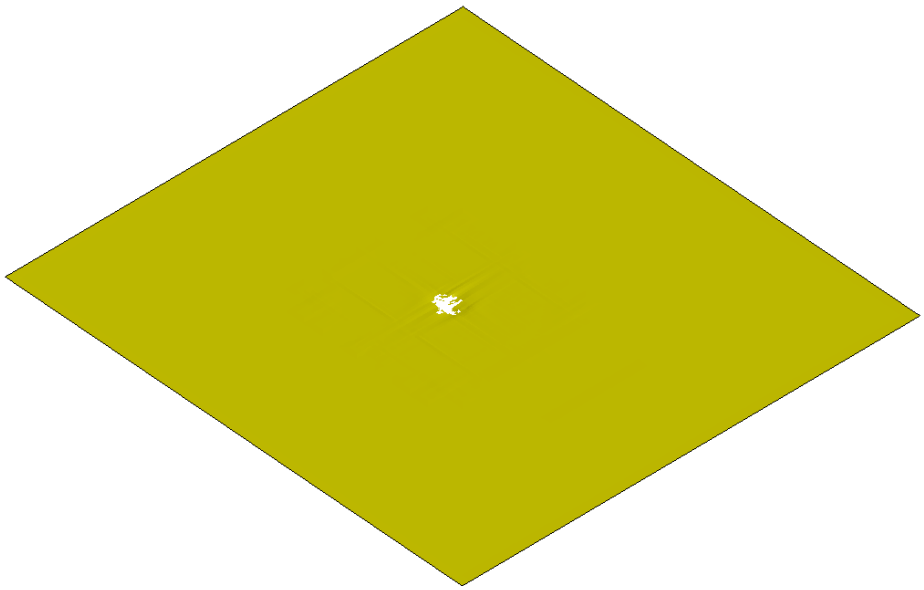

(c) GN2118 layer damage

Figure 4-11: Knife and target material model at 75% penetration depth

During the FEA analysis of this model, there were problems in the contact definition of the knife to the composite materials causing the FE analysis to stop due to instabilities and large element deformations. This was most likely due to the sharp-end-geometry of the knife and the complex composite material.

Table 4-4 shows some of the runs for this model and it can be seen that none of the runs show a complete penetration of the knife into the target material. Hence a new contact definition had to be defined in order to obtain FEA results that showed a through penetration of the target material.

Table 4-4: Approach 1 knife test calibration runs and results

Run #	Material	Shear Strength	Transverse Compression Strength	Shear Modulus	Time-step before distortion (ms)	Tip of knife Displacement (mm)
1	GN2118	$1x10^{-3}$	$5 x10^{-6}$	0.292	1.7	3.5
	AS299	$1x10^{-3}$	$1 x10^{-5}$	0.145		
2	GN2118	$1x10^{-3}$	$5 x10^{-6}$	2.92	0.6	1.03
	AS299	$1x10^{-3}$	$1 x10^{-5}$	1.45		
3	GN2118	$3x10^{-4}$	$5 x10^{-6}$	0.00292	No failure	7.1
	AS299	$1x10^{-4}$	$1 x10^{-5}$	0.00145		
4	GN2118	$1x10^{-3}$	$5 x10^{-4}$	2.92	0.9	1.54
	AS299	$1x10^{-3}$	$1 x10^{-3}$	1.45		
5	GN2118	$2x10^{-3}$	$5 x10^{-6}$	0.292	3.1	2.7 (rebounds at 2.0ms)
	AS299	$2x10^{-3}$	$1 x10^{-5}$	0.145		
6	GN2118	$1x10^{-3}$	$5 x10^{-6}$	0.292	1.4	2.3 mm
	AS299	$8x10^{-4}$	$1 x10^{-5}$	0.145		
7	GN2118	$5x10^{-4}$	$5 x10^{-6}$	0.292	0.4	0.79
	AS299	$1x10^{-4}$	$1 x10^{-5}$	0.145		

4.8 Knife model test results using Approach Two Model

In the second approach automatic surface to surface was defined for the different layers of the target material, which includes GN2118, AS299, foam, and steel plate. To define contact between the knife and target materials, nodes along the center of the target material where the knife makes contact were tied based on plastic strain failure criteria. In order to tie the nodes additional nodes were defined in the four elements forming a corner as shown in Figure 4-12 below. Figure 4-13 below shows the line with the tied nodes where the knife and target material makes contact. The plastic failure strain used as an input value was varied along with the material properties that are not known.

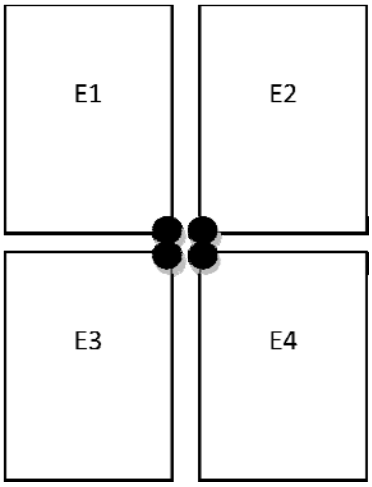

Figure 4-12: Tied element in the target material

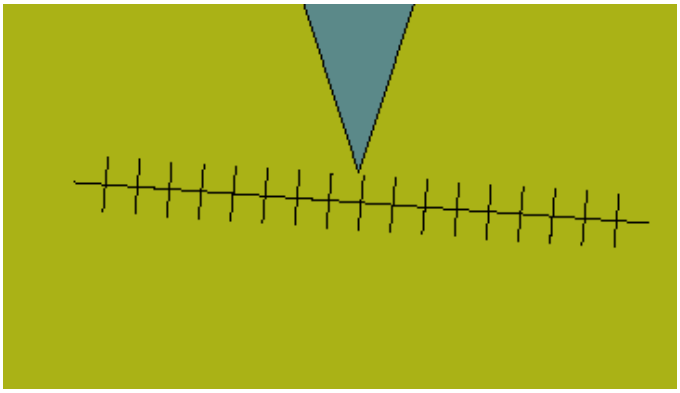
Figure 4-13: Additional nodes defined for a tied corner of four elements

Table 4-5 below shows the different runs and results with varied material properties. The subscripts for the shear modulus correspond to the element directions of the composites (i.e. AB is equivalent to the local xy direction of the composite element, BC is equivalent to the yz direction, and CA is equivalent to the zx direction). The velocities shown correspond to a positive upward velocity achieved after the knife penetrates and then rebounds upwards. The results show that the plastic failure strain did not vary the final velocity and penetration depth. Shear strength, transverse compressive strength, and shear modulus were the main factors that contributed to various final velocities and penetration depths for the second approach model. It is difficult to achieve a zero velocity and no knife rebound since more specific material properties of GN2118 and AS299 need to be studied and known. The runs might also be a function of the global damping coefficient which for this approach was not varied. For zero or very low shear modulus values in xz, and yz direction the highest penetration was observed. Finally, it can be seen that for both runs 1 and 2 the depth of penetration is 9.6 mm which is greater than the total FEA thickness of the fabric samples of 7.3 mm. Thus for these two runs, the penetration was larger than fabric thickness but the knife velocity did not approach zero. The positive values of the final velocity correspond to the upward velocity of the knife after it rebounded.

Table 4-5: Approach 2 knife test calibration runs and results

Run #	Material	Plastic Failure Strain	Shear Strength ($x10^9$ Pa)	Transv. Comp. Strength ($x10^9$ Pa)	Shear Modulus G_{AB}, G_{BC}, G_{CA} ($x10^9$ Pa)	Final Velocity (mm/ ms)	Penet. Depth (mm)
1	GN2118	0.024	1	0.1	15, 0, 0	>4.5	9.575
	AS299	0.03	0.1	0.2	10, 0, 0		
2	GN2118	0.05	1	0.1	15, 0, 0	>4.5	9.574
	AS299	0.08	0.1	0.2	10, 0, 0		
3	GN2118	0.024	2	1	15, 15, 15	0.5	0.97
	AS299	0.03	1.1	2	10, 10, 10		
4	GN2118	0.024	2	0.5	15, 15, 15	0.5	0.97
	AS299	0.03	1.1	1	10, 10, 10		
5	GN2118	0.024	1	0.5	15, 15, 15	0.58	0.97
	AS299	0.03	0.1	1	10, 10, 10		
6	GN2118	0.024	0.02	0.001	0.15, 0.015, 0.015	> 0.3	1.2
	AS299	0.03	0.01	0.002	0.1, 0.01, 0.01		

5. CONCLUSIONS AND FUTURE WORK

5.1 Conclusions

The following summarizes the research done in body armor testing and modeling:

1. Light, ultra-concealable body armor which protects not only against stab armor but also ballistic threats requires materials that are flexible, have a very high strength to weight ratio and are thin and flexible.
2. Materials such as AS299 and AS400 that are Kevlar woven materials impregnated with resin epoxy, demonstrate the highest resistance to stab threats. GN2118, a Kevlar based material, has been used during the testing and modeling procedure primarily to stop ballistic threats only.
3. A configuration using both AS299 and AS400 layers of materials is more effective against spike and knife threats.
4. Experimental test have been conducted to obtain material properties necessary to model the knife penetration using FEA. This included tensile tests for the fiber-resin fabrics and compression test for foam which is used as a backing material.
5. While there are many material models to model composite materials, the orthotropic material model with in plane stress assumptions is used to model GN2118 and AS299. Low density foam is used to model the foam backing material.
6. In order to validate the different material models for an impact test such as the knife test, a drop sphere test was conducted. This test involved a steel

sphere with known material properties. The measured bounce height experimentally was matched to the FEA results by calibrating the damping coefficient.

7. Preliminary work using FEA has been done to model the knife penetration into fabric. Geometry of knife, boundary conditions, and energy requirements have been defined to closely match the NIJ knife test. The results obtained using tied nodes method show good correlation between the depth of penetration using the FEA model and experimental results. However, the final velocity could not be matched closely due to limitations in the LS-DYNA composite material models and the lack of some experimental data. Automatic contact between fabrics and knife did not give good results due to the complicated geometry of the knife and contact definitions.

5.2 Future Work

- In the studies, it has been noticed that the shear and compression material properties are very important in modeling the shearing effect of the knife on the composite materials. Hence, shearing and compression tests need to be done on these materials.
- In order to better compare the experimental and FEA results of the knife test, the impact energy of knife on the material needs to be measured.

REFERENCES

[1] NIJ Standard 0115.00 “Stab resistance of personal body armor” National Institute of Justice, Sept 2000.

[2] C.T. Nguyen, T. Vu-Khanh, and J. Lara. "Puncture characterization of rubber membranes." Theoretical and Applied Fracture Mechanic 2004; 42: 25-33.

[3] "Standard Test Method for Protective Clothing Material Resistance to Puncture." ASTM Standard F1342-05.

[4] D.C. Erlich, D.A. Shockey, and J.W. Simons. "Slow penetration of ballistic fabrics." Textile Research Journal, 2003; 73, 2: 179-184.

[5] H.S. Shin, D.C. Erlich, and D.A. Shockey. "Test for measuring cut resistance of yarns." Journal of Materials Science .2003; 38: 3603-3610.

[6] R.F. Wilson-Fahmy, D. Narejo, and R.M. Koerner. "Puncture protection of geomembranes, Part I: Theory." Geosynthetics International 3, 1996, no. 5: 605-628.

[7] T.K. Ghosh. "Puncture resistance of pre-strained geotextiles and its relation to uniaxial tensile strain at failure." Geotextiles and Geomembranes 16, 1998, no. 5: 293-302.

[8] "Standard Test Method for Measuring Cut Resistance of Materials Used in Protective Clothing." ASTM Standard F1790-05.

[9] J. Lara, D. Turcot, R. Daigle, and J. Boutin. "New test method to evaluate the cut resistance of glove materials." ASTM Special Technical Publication 1996; 1237: 23-31.

[10] J. Lara, D. Turcot, R. Daigle, and F. Payot. "Comparison of two Methods to evaluate the resistance of protective gloves to cutting by sharp blades." ASTM Special Technical Publication, 1996; 1237: 32-42.

[11] J. Lara and S. Masse. Evaluating the cutting resistance of protective clothing materials. Proceedings of 1st European Conference on Protective Clothing, Stockholm, Sweden, May 7-10, 2000, edited by Kalev Kuklane and Ingvar Holmer 145-149.

[12] S.S. Deshmukh and G.H. McKinley. Adaptive energy-absorbing materials using field-responsive fluid-impregnated cellular solids. Smart Materials and Structures, 2007; Volume 16, Number 1.

[13] R. Gadow and K. von Niessen."Lightweight Ballistic with Additional Stab Protection Made of Thermally Sprayed Ceramic and Cermet Coatings on Aramide Fabrics." Journal of Applied Ceramic Technology 3, 2006, no. 4: 284-292.

[14] S.R. Raghavan and S.A. Khan. "Shear-induced microstructural changes in flocculated suspensions of fumed silica," Journal of Rheology 39, 1995, no. 6: 1311-1325.

[15] S.R. Raghavan and S.A. Khan. "Shear-Thickening Response of Fumed Silica Suspensions under Steady and Oscillatory Shear," Journal of Colloid and Interface Science, 1997; 185: 57-67.

[16] B.J. Maranzano and N.J. Wagner. "The effects of particle size on reversible shear thickening of concentrated colloidal dispersions," Journal of Chemical Physics, 2001; 114, no. 23: 10514-10527.

[17] Y.S. Lee and N.J. Wagner. "Dynamic properties of shear thickening colloidal suspensions," Rheology Acta 42, 2003; no. 3: 199-208.

[18] Y.S. Lee, Wetzel, E.D. and N.J. Wagner. "The ballistic impact characteristics of Kevlar® woven fabrics impregnated with a colloidal shear thickening fluid," Journal of Materials Science 38, 2003; no. 13: 2825- 2833.

[19] Y.S. Lee, E.D. Wetzel, R.G. Egres Jr., and N.J. Wagner. Advanced Body Armor Utilizing Shear Thickening Fluids. Proceedings of the 23rd Army Science Conference, 2002.

[20] E.D. Wetzel, Y.S. Lee, R.G. Egres, K.M. Kirkwood, J.E. Kirkwood, and N.J. Wagner. Proceedings of NUMIFORM, 2004.

[21] R.G. Egres, Y.S. Lee, J.E. Kirkwood, K.M. Kirkwood, E.D. Wetzel and N.J. Wagner. Proceedings of the 14th International Conference on Composite Materials, July 2003.

[22] R.G. Egres Jr., M.J. Decker, C.J. Halbach, Y.S. Lee, J.E. Kirkwood, K.M. Kirkwood, E.D. Wetzel, N.J. Wagner. Stab Resistance of Shear Thickening Fluid (STF)-Kevlar Composites for Body Armor

Applications. In Proceedings of the 24th Army Science Conference, Orlando, Florida, November 29-December 2, 2004.

[23] V.B.C. Tan, T.E. Tay and W.K. Teo. "Strengthening fabric armour with silica colloidal suspensions," International Journal of Solids and Structures, 2005; 42: 1561-1576.

[24] R. W. Buckley. Polymer Enhancement of Technical Textiles. © Smithers Rapra. Shrewsbury, GBR, 2003

[25] S.L. Phoenix and P.K. Porwal.. "A new membrane for the ballistic impact response and V50 performance of multi-ply fibrous systems," International Journal of Solids and Structures, 2003; 40: 6723- 6765.

[26] P.K. Porwal and S.L. Phoenix. "Modeling system effects in ballistic impact into multi-layered fibrous materials for soft body armor," International Journal of Fracture, 2005; 135: 217-249.

[27] W.J. Taylor and J.R. Vinson.. "Modeling Ballistic Impact into Flexible Materials," American Institute of Aeronautics and Astronautics 28, 1989; no.12: 2098-2103.

[28] S. Luo and T. Chou. "Finite Deformation of Flexible Composites," Proceedings of the Royal Society of London 429, 1990; no.1877: 569-586.

[29] S. Suresh, A.E. Giannakopoulos and J. Alcala. "Spherical Indentation of Compositionally Graded Materials: Theory and Experiments," Acta Metallurgica 45, 1997; no.4: 1307-1321.

[30] S. Suresh and A.E. Giannakopoulos. "A New Method for Estimating Residual Stresses by Instrumented Sharp Indentation," Acta Metallurgica 46, 1998; no. 16: 5755-5767.

[31] A.E. Giannakopoulos and S. Suresh. "Determination of Elastoplastic Properties by Instrumented Sharp Indentation," Scripta Materialia 40, 1999; no. 10: 1191-1198.

[32] E.W. Andrews; A.E. Giannakopoulos; E. Plisson, and S. Suresh. "Analysis of the impact of a sharp indenter," International Journal of Solids and Structures 39, 2002; no. 2: 281-295.

[33] J. Sharda, C. Deenadayalu, B. Mobasher and S. D. Rajan, "Modeling of

Multi-Layer Composite Fabrics for Gas Turbine Engine Containment Systems", ASCE J of Aerospace Engineering, 2006; 19:1, 38-45.

[34] D. Naik, S. Sankaran, B. Mobasher, S. D. Rajan, J. M. Pereira, "Development of Reliable Modeling Methodologies for Fan Blade-Out Containment Analysis. Part I: Experimental Studies", J of Impact Engineering , 2009; 36:1, 1-11.

[35] Z. Stahlecker, B. Mobasher, S.D. Rajan, J. M. Pereira, "Development of Reliable Modeling Methodologies for Fan Blade-Out Containment Analysis. Part II: Finite Element Analysis", J of Impact Engineering, 2009; 36:3, 447-459.

[36] S. Bansal, B. Mobasher, S.D. Rajan, I. Vintilescu, "Numerical Modeling of Engine Fan Blade-Out Events", ASCE J of Aerospace Engineering, 22, 249-259, 2009.

[37] S.D. Rajan, B. Mobasher, "A Comprehensive Methodology for Characterization of Dry Fabrics", World Journal of Engineering, 2010; 7:1, 154-162.

[38] R.E. Walpole, R.H. Myers. Probability and Statistics for Engineers and Scientists. Fifth edition. Macmillan Publishing Company. New York. 1993

[39] D.C. Montgomery. Design and Analysis of Experiments. 5th edition. John Copyright © 1997, 2007 John Wiley & Sons. Inc.

[40] D.C. Montgomery, C. L. Jennings, M. Kulahci. Introduction to Time Series Analysis and Forecasting. Copyright © 2008 John Wiley & Sons. Inc.

[41] A. Savitzky, M. J.E. Golay. Smoothing and Differentiation of Data by Simplified Least Squares Procedures. The Perkin-Elemer Corp., Norwalk, Conn, 1964; Vol. 36, No.8, July.

[42] E.W. Weisstein. "Least Squares Fitting—Polynomial." From MathWorld—A Wolfram Web Resource. Access date: 12/1/2011 http://mathworld.wolfram.com/LeastSquaresFitting Polynomial.html

[43] H. Motulsky, A. Christopoulos. Fitting Models to Biological Data Using

Linear and Nonlinear Regression. Oxford University Press. GraphPad Software, Inc. 2004.

[44] E. Oberg, F.D. Jones, C. J. McCauley, R.M. Heald (2008), Machinery's Handbook (28th ed.), Industrial Press.

[45] B. Croop, H. Lobo (2009). "Selecting Material Models for the Simulation of Foams in LS-DYNA". 7th European LS-DYNA Conference. DatapointLabs, NY USA.

[46] Honeywell Specialty Materials. "Honeywell Gold Shield® GN-2118 with Kevlar® ballistic composite material." ©2010 Honeywell International Inc. Web access data 11/25/2011. http://www51.honeywell.com/sm/afc/products-details/shield.html

[47] ASTM Standard D 3039 (2008a). "Standard Test Method for Tensile Properties of Polymer Matrix Composite Materials," ASTM International, West Conshohocken, PA.

[48] ASTM Standard D 1056. "Standard Specification for Flexible Cellular Materials – Sponge or Expanded Rubber" ASTM International, 2008a. West Conshohocken, PA.

[49] K.K Chawla. Composite Materials, 2nd Edition. Springer Science. ©1998

[50] Stahlecker, Z., Mobasher, B., Rajan, S.D. and Pereira, J.M. "Development of reliable modeling methodologies for fan blade-out containment analysis. Part II: finite element analysis," J of Impact Engineering, 2009; 36:3, 447-45.

[51] E. Young. SolidWorks Education Edition. Dessault Systémes. Copyright© 1995-2009

[52] Altair Engineering Inc. Altair®, HyperMesh®. Version 11.0. A Platform for Innovation ™. Copyright 1986-2011

[53] LS-DYNA, Theory Manual. Livermore Software Technology Corp., Livermore CA, 2006.

[54] LSTC Inc. DYNAmore. Engineering Research Nordic AB. "Contact Types". November 8, 2011. http://www.dynasupport.com/tutorial/contact-modeling-in-ls-dyna/contact-types

APPENDIX A

EXAMPLES OF DATA ANALYSIS

A.1 Determining number of replicates to be tested

Table 0-1 shows a set of four foam samples with similar cross-sectional areas prepared for compression testing.

Table 0-1: Choice of Sample Size Data with One Parameter Design

	Observations		
Sample	1	2	3
1	939	921	902
2	863	876	860
3	889	888	891
4	928	910	858

Approximating that the maximum mean difference between any of the cross-sectional areas of the sample should not be greater than 9 mm^2, the standard deviation is approximately 30, the alpha value is 0.05, and the a probability of rejecting null hypothesis is 90 percent, the number of replicates is calculated as shown below.

For n = 3:

$$\Phi^2 = \frac{3 \cdot 18^2}{2 \cdot 4 \cdot 25^2} = 3.24$$
$$\Phi = 1.8 \qquad (4.3)$$

The probability of accepting the null hypothesis can be found from the operating characteristic curves for the fixed effects model analysis of variance, as in the Design and Analysis of Experiments book by Douglas Montgomery Appendix V. Using $\Phi = 1.8$, $\alpha = 0.05$, and numerator degree of freedom of $a - 1 = 4 - 1 = 3$ and denominator degrees of freedom of $a(n-1) = 4(3-1) = 8$, the probability of the null hypothesis being rejected is $1 - \beta = 1 - 0.39 = 0.61$.Since 0.61 is less than 0.9,

null hypothesis is not rejected, hence the number of samples needs to be greater than 3.

For n = 4:

$$\Phi^2 = \frac{4 \cdot 18^2}{2 \cdot 4 \cdot 25^2} = 6.48$$
$$\Phi = 2.54 \qquad (4.4)$$

Using the operating characteristic curves, $\Phi = 1.8$, $\alpha = 0.05$, and numerator degree of freedom of $a - 1 = 4 - 1 = 3$ and denominator degrees of freedom of $a(4-1) = 4(4-1) = 12$, the probability of the null hypothesis being rejected is $1 - \beta = 1 - 0.04 = 0.96$.Since 0.96 is greater than 0.9, null hypothesis is rejected and hence the number of samples needed to fulfill the given requirements is 4.

The same theory applies if more than one factor is involved in deciding the number of samples. Examples of multiple factor choice of sample size may be found in section 5-3.5 of the Douglas C. Montgomery Design and Analysis of Experiments book.

A.2 Smoothing and best-fitting data

Data from uniaxial testing one sample of GN2118 is presented below. The raw data obtained from the test include time, displacement, and load. The engineering stress and strain is calculated as described in section 3.1. The testing results are presented graphically in Figure 0-2: and some of the recorded data is shown in

Table 0-2:. The average sample dimensions used to convert load-displacement data to stress-strain data are

$$L_{Gage} = 8.0in \tag{4.5}$$

$$Width = 1.4625in \tag{4.6}$$

$$Thickness = 0.00475in \tag{4.7}$$

From the above dimensions, the average cross-sectional are is

$$A_{avg} = 1.4625x0.00475 = 0.006947in^2 \tag{4.8}$$

The stress and strain calculation for the second point in the raw recorded data from the uniaxial test is shown below.

$$\sigma_2 = \frac{2.08816}{0.006947} = 300.589\,psi \tag{4.9}$$

$$\varepsilon_2 = \frac{0.00085298}{8.0} 0.000107 \tag{4.10}$$

Table 0-2: Load-displacement and stress-strain data from a uniaxial tension test of a GN2118 sample

Displacement (in)	Load (lb)	Strain (in/in)	Stress (psi)
0	0	0	0
0.00085298	2.088157	0.000107	300.5893
0.00165678	5.731046	0.000207	824.9819
0.00249378	9.242345	0.000312	1330.432
□	□	□	□
0.14168004	516.1286	0.01771	74296.52
0.1425178	517.8939	0.017815	74550.63
0.14335764	517.1468	0.01792	74443.08
0.14421552	516.9928	0.018027	74420.91
0.14502738	517.7893	0.018128	74535.57
0.14586664	518.2828	0.018233	74606.61
0.1467075	518.8219	0.018338	74684.22
0.14753611	519.4908	0.018442	74780.5
□	□	□	□
0.19772608	17.82867	0.024716	2566.43
0.19855952	17.68479	0.02482	2545.718
0.19937918	16.27944	0.024922	2343.419
0.20023684	1.34346	0.02503	193.3905
0.20104303	0.761703	0.02513	109.6468
0.20192554	0.465768	0.025241	67.04718

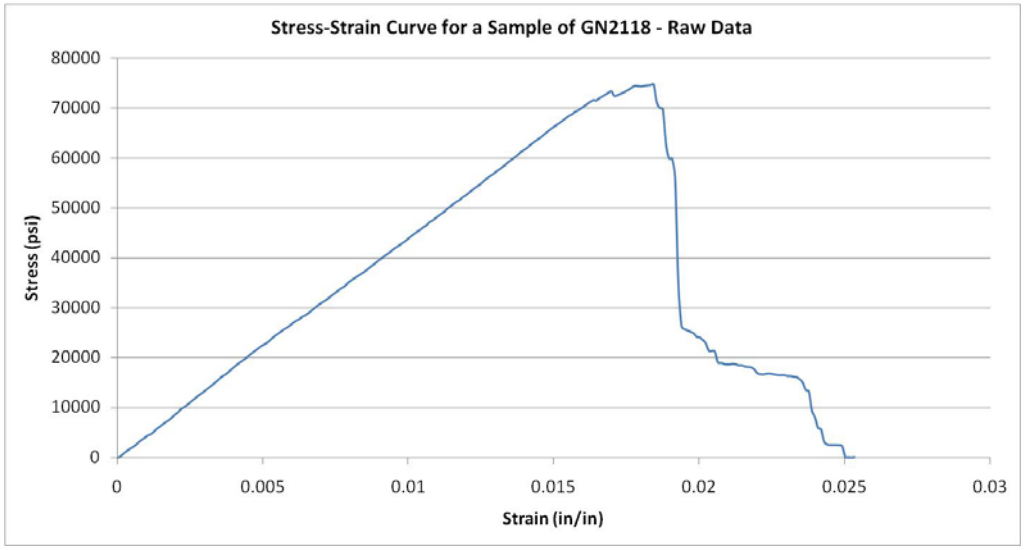

Figure 0-1: Stress-strain curve for a sample of GN2118 – Raw Data

The above data can be smoothed using the simple moving average. This technique explained in detail in section 0 was defined as

$$Y_j = \frac{\sum_{i=-m}^{i=m} Y_{j+i}}{N} \tag{4.11}$$

To show how the above formula is implemented for five-point smoothing the calculations for the new smoothed value of the third point in the stress-strain raw data is shown below.

$$Y_3 = \frac{0.0 + 300.59 + 824.98 + 1330.43 + 1749.45}{5} = 1265.71 \tag{4.12}$$

The smoothed data is provided in Table 0-3 below and shown graphically in Figure 0-2:.

Table 0-3: Smoothed stress-strain data from a uniaxial tension test of a GN2118 sample

Strain	Stress	Smoothed Data
0	0	0
0.000107	300.5893	300.5893
0.000207	824.9819	841.0915
0.000312	1330.432	1265.705
□	□	□
0.01771	74296.52	74133.44
0.017815	74550.63	74312.8
0.01792	74443.08	74449.34
0.018027	74420.91	74511.36
0.018128	74535.57	74538.08
0.018233	74606.61	74605.56
0.018338	74684.22	73980.15
0.018442	74780.5	73090.53
□	□	□
0.024716	2566.43	2522.994

0.02482	2545.718	2046.295
0.024922	2343.419	1551.721
0.02503	193.3905	1051.844
0.02513	109.6468	109.6468
0.025241	67.04718	67.04718

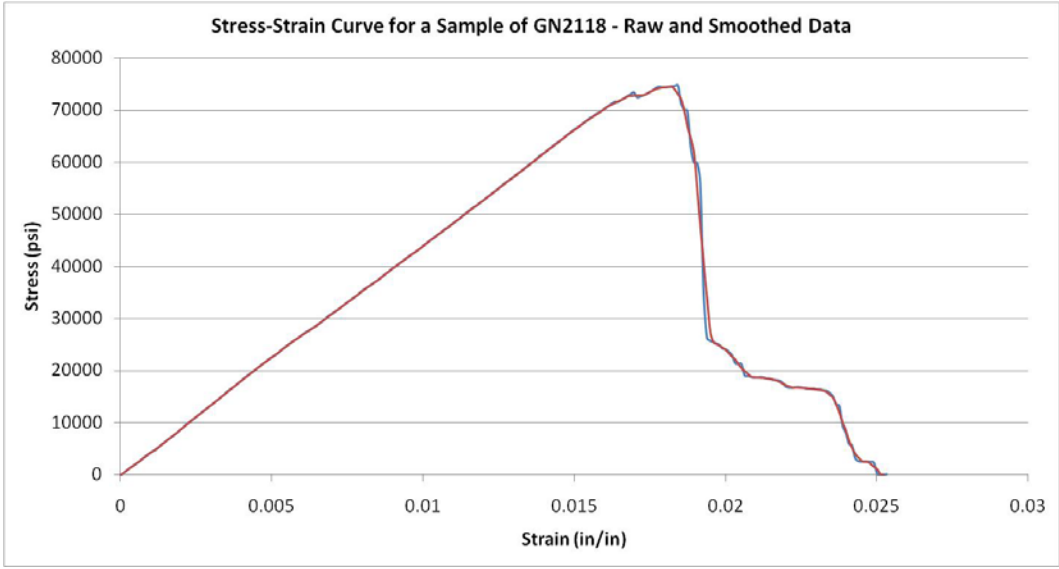

Figure 0-2: Stress-strain curve for a sample of GN2118 – raw and smoothed Data

If a linear polynomial is fit to the above pre-peak smoothed data, the best fit line is found to be:

$$y = 4{,}397{,}111.48x + 137.52 \tag{4.13}$$

Some of the smooth data substituted into equation (2.17) is shown below.

$$\begin{bmatrix} 1 & 0.0 \\ 1 & 0.000107 \\ 1 & 0.000207 \\ 1 & 0.000312 \\ 1 & \vdots \\ 1 & 0.017815 \\ 1 & 0.01792 \\ 1 & 0.018027 \end{bmatrix} \begin{bmatrix} a_0 \\ a_1 \end{bmatrix} = \begin{bmatrix} 0 \\ 300.5893 \\ 841.0915 \\ 1265.705 \\ \vdots \\ 74312.8 \\ 74449.34 \\ 74511.36 \end{bmatrix} \tag{4.14}$$

The regression coefficients from solving the above equation are found to be

$$a_0 = 137.52$$
$$a_1 = 4,397,111.48 \tag{4.15}$$

Referring to equations (2.30) , (2.31), and (2.32) the R-squared value is calculated by calculating the sum of squares of the vertical distance of the points from the best-fit curve, SS_{reg}, and the sum of squares of the vertical distance of the points from a horizontal line through the mean of all Y values, SS_{tot}. Using data software such as Microsoft Excel we calculate

$$SS_{REG} = 6,900,065$$
$$SS_{TOT} = 6.1436(10)^{10} \tag{4.16}$$

Calculating the regression coefficient

$$R^2 = 1 - \frac{6,900,065}{6.1436(10)^{10}} = 0.999 \tag{4.17}$$

A value this close to 1.0 can lead to a conclusion that the linear regression fit for the above set of data, is a good one.

APPENDIX B

MATERIAL DAMAGE FROM KNIFE AND SPIKE TESTING

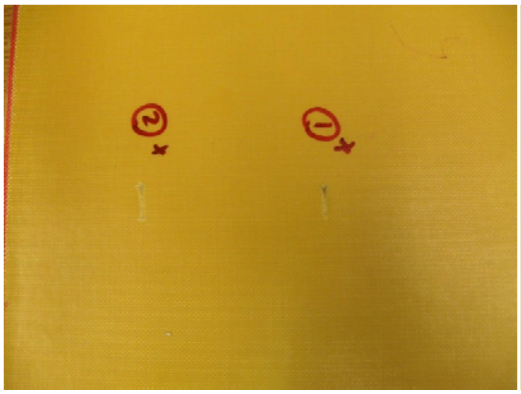

(a) Layer 1

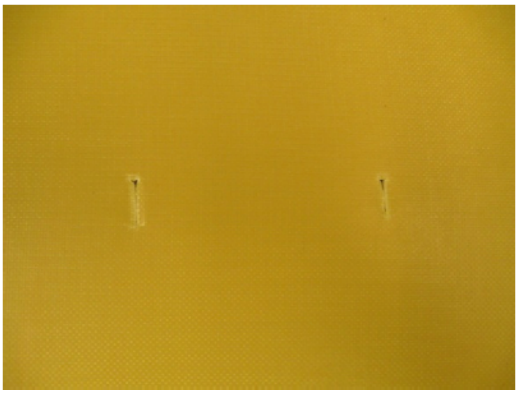

(b) Layer 10

(c) Layer 20

(d) Layer 30

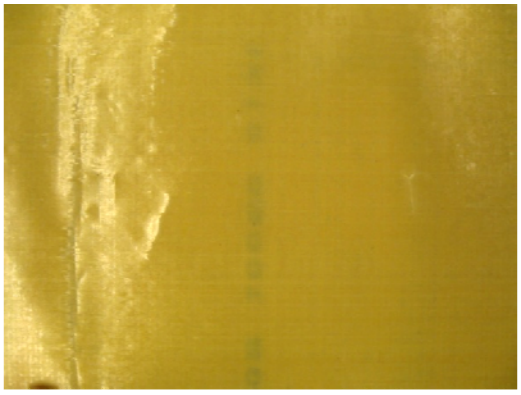

(e) Layer 40

Figure 0-1: Knife testing results for sample 1 – (a) to (c) Damage of AS299, (d) to (e) Damage of GN2118

Sample 2 Sample results

(a)Layer 1 (b) Layer 10

(c)Layer 20 (d) Layer 30

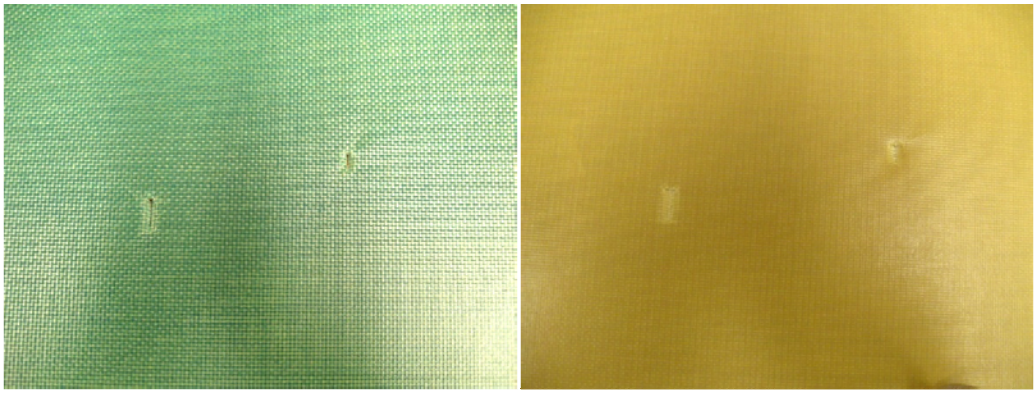

(e)Layer 38 (f) Layer 50

Figure 0-2: Knife testing results for sample 2 – (a) to (c) Damage of GN2118, (d) and (f) Damage of AS299, (e) Damage of AS400

APPENDIX C

ENGINEERD KNIFE AND SPIKE

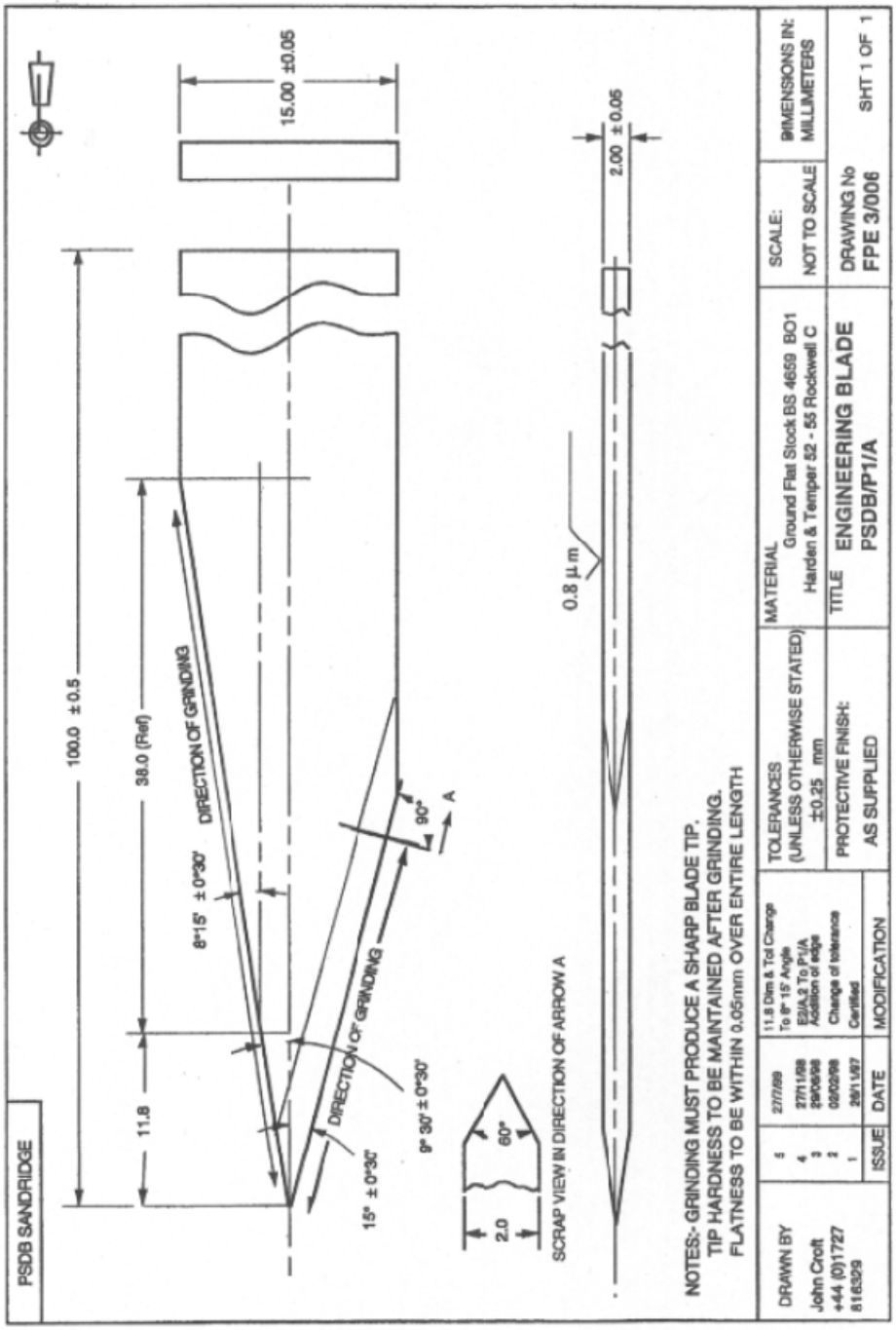

Engineered Knife Blade P1

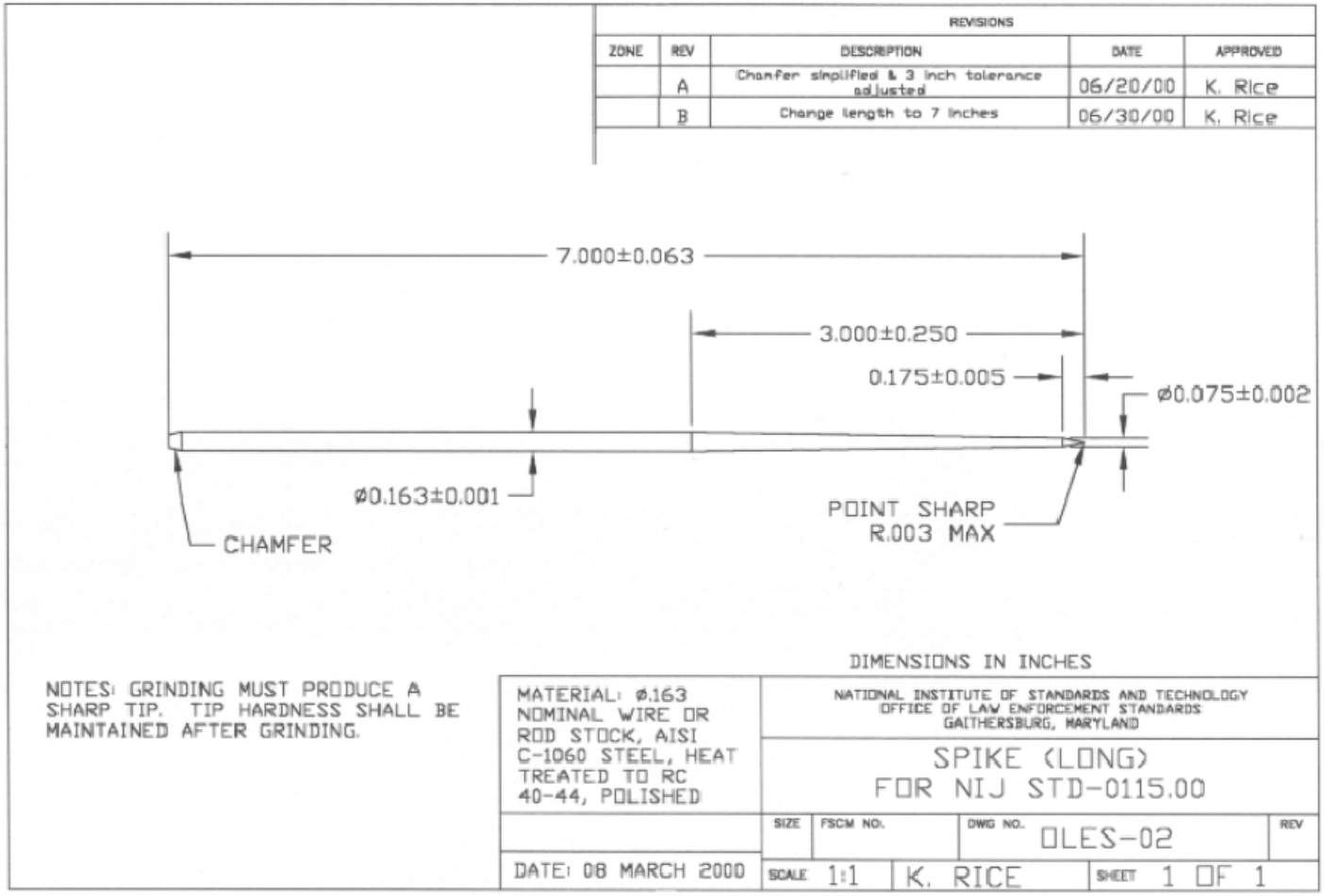

Engineered Spike